Revision 1

Role of volatiles (S, Cl, H_2O) and silica activity on the crystallization of haüyne and nosean in phonolitic magmas (Eifel, Germany and Saghro, Morocco)

Céline Baudouin* and Fleurice Parat

Géosciences Montpellier, UMR 5243 - CC 60 - Université Montpellier, Place E. Bataillon, 34095 Montpellier cedex 5, France

***Corresponding author: Céline Baudouin**

Tel.: +33 4 67 14 39 39; Fax +33 (0) 4 67 14 36 42

E-mail: celine.baudouin@gm.univ-montp2.fr

Abstract

To constrain the crystallization of alkaline and volatile-rich lavas present in intraplate settings, we studied the petrological features and the geochemical composition of major, trace and volatile elements of mineral and bulk-rock of two sodalite-bearing phonolites: (i) haüyne-plagioclase-bearing Si-K-rich phonolite from Laacher See (Germany) and (ii) nosean-nepheline-bearing Si-poor phonolite from Saghro (Morocco). In haüyne-bearing phonolites (55-59 wt% SiO_2, K>Na, Na+K/Al =0.96-1.08), we found that the low silica and low sodium activity promoted the early crystallization of S-rich haüyne (13.7-13.9 wt% SO_3, 0.4 wt% Cl) + S-rich apatite (0.7-0.9 wt% SO_3), titanite and rare pyrrhotite followed by clinopyroxene-plagioclase-sanidine at relatively low pressure and temperature (P=250 MPa and T=850 °C) and oxidized condition (ΔNNO-NNO+1, where NNO is nickel-nickel oxide buffer). The crystallization of haüyne occurred at fluid-undersaturated conditions from a silicate melt with 6 wt% H_2O, 0.17-0.55 wt% Cl, 0.11-0.4 wt% S and 0.07-0.14 wt% F. Nosean-bearing phonolites from Saghro are silica-poor and peralkaline (52-54 wt% SiO_2, Na>K, Na+K/Al =1.2) and crystallized at higher P and T (300 MPa and 950 °C) and more reduced conditions (NNO) compared to haüyne-bearing phonolites. The incongruent reaction to form nosean requires high silica and Na_2O activity. The mineral assemblage and composition suggest early crystallization of nepheline followed by nosean (7.8-8.8 wt% SO_3; 1-1.1 wt% Cl). The sequence of crystallization is: clinopyroxene + nepheline + S-poor apatite (<0.04 wt% SO_3) + pyrrhotite followed by nosean and titanite. Nosean-bearing magmas are fluid-undersaturated with relatively low volatile content (4 wt% H_2O, <0.25 wt% Cl, <0.056 wt% S, 0.08-0.1 wt% F), although Cl may have exsolved during ascent and formed a fluid phase (NaCl-bearing).

Both haüyne- and nosean-bearing phonolites are last equilibrated at relatively low pressure and high temperature. Haüyne and nosean crystallized at oxidized and volatile-rich

pre-eruptive conditions. They record the volatile concentrations at depth and may be used as oxybarometer. The incongruent reactions involved to form haüyne and nosean suggest that phonolitic magmas became more oxidized during crystallization. The initial volatile concentrations in basanite/nephelinite magmas, from partial melting of volatile-bearing K_2O-rich mantle rock, should have been one important factor influencing the crystallization of haüyne-bearing Si-K-rich phonolite and nosean-bearing Si-poor phonolite in intracontinental setting.

Key words:

Phonolite, sodalite, haüyne, nosean, volatile elements, pre-eruptive conditions

Introduction

In alkaline and silica undersaturated volcanic rocks, the presence of minerals of the sodalite group (volatile-bearing feldspathoid mineral $Na_8(AlSiO_4)_6(Cl_2, SO_4)$ attests to the presence of volatile in magmas and possible deep magmatic fluids in both oceanic (e.g. Cape Verde: Holm et al. 2006, Canary island: Bryan 2006) and continental intraplate setting (Brousse et al. 1969; Wörner and Schmincke 1984a; DeFino et al. 1986). Sodalite minerals are phenocrysts and incorporate volatile elements such as Cl and S. They are therefore key minerals to characterize volatile concentrations and speciation at pre-eruptive conditions, constrain the behavior of volatile elements during magma differentiation and ascent (e.g. crystallization and degassing) and address the question of the role and origin of volatile elements in alkaline magma genesis.

Sodalite minerals have been reported in mafic and felsic alkaline magmatic rock compositions from tephrite to phonolite, but are predominantly present in phonolite (review in Parat et al. 2011). Phonolites are alkali-rich and silica-rich magmas and the processes involved for their genesis are still under debated including (i) fractionational crystallization from low-silica melts, with nephelinite, basanite and melilitite primary compositions (Edgar 1987; Thompson et al. 2001; Wedepohl et al. 1994; Wörner and Schmincke 1984b), (ii) direct melting or fractionating of the mantle (Price and Green 1972; Bailey 1987; Laporte et al. 2014), or (iii) remelting of basanite (Legendre et al. 2005).

Phonolites can erupt explosively or form extrusive dome as a result of variable volatile concentration at depth. However, published data on volatile concentrations and speciations are scarce. Interestingly, among sodalite-bearing phonolites, we identified two groups: (1) Si-rich phonolite with haüyne (Wörner and Schmincke 1984a; Holm et al. 2006; Bryan 2006) and (2) Si-poor phonolite with nosean (Brousse et al. 1969; Berger et al. 2009) or only sodalite (Klaudius and Keller 2006; Zaitsev et al. 2012) (Figure 1).

These two groups of phonolites with haüyne or nosean represent a unique opportunity to constrain the condition of crystallization of sodalite minerals in natural environments. We selected two samples, one with haüyne and one with nosean, and investigated in detail the mineralogy and geochemistry: (1) haüyne-bearing Si-rich phonolite, a tephra from Laacher See (Eifel, Germany) and (2) nosean-bearing Si-poor phonolite, a lava dome from Saghro volcanic field, Morocco (Figure 1). We combine an extensive multi-method geochemical study of major, minor, trace elements including volatile elements in sodalite, silicate minerals, apatite, titanite, pyrrhotite and bulk rock. We determined the phase assemblage, mineral-melt equilibrium, and volatile concentration and speciation in phonolite at depth and constrained the pre-eruptive conditions and the crystallization environment of phonolitic magmas in intracontinental settings.

I. Sodalite group minerals in magmatic rocks

Sodalite (cubic, *P*43*n*) is a high temperature, low-pressure mineral, crystallizing well above the solidus in sodic silica-undersaturated magmas enriched in NaCl, and its presence constrains NaCl activities in magmas (Sharp et al. 1989). Sodalite group minerals are alkali- and volatile-bearing mineral with solid solutions evolving between 4 end-members: Na-Ca(-K) end-members and Cl-S end-members $Na_8(AlSiO_4)_6(Cl_2, SO_4)$ - $(Na,Ca)_{4-8}(AlSiO_4)_6(SO_4,S)$ (Tomisaka and Eugster 1968): sodalite (Na-Cl sodalite), nosean (Na-S-Cl sodalite) and haüyne (Na-Ca-S sodalite). Only few experimental and thermodynamic studies have been performed to constrain the stability of sodalite group minerals at high pressure and high temperature (Tomisaka and Eugster 1968; Stormer and Carmichael 1971). They showed that a complete solid solution exists between nosean and haüyne at 600°C and 100 MPa, whereas the solid solution sodalite–nosean and sodalite-haüyne is limited, as Cl^- and SO_4^{2-} substitute

with much more difficulty than Ca^{2+} and Na^{+} (Van Peteghem and Burley 1963). The presence of volatile elements such as S and Cl as well as H_2O and CO_2 in haüyne (up to 1 and 0.75 wt%, respectively, Bellatreccia et al. 2009) in the structural cavities of the mineral is directly linked to the composition of magmatic silicate liquid from which they crystallized. Thus, determining the composition of sodalite constraints the composition of magma from which they crystallized and the concentration of volatile at depth.

The stability of sodalite $Na_8(AlSiO_4)_6(Cl_2, SO_4)$ has been examined using thermodynamic equilibrium (Stormer and Carmichael 1971). The sodalite crystallization is related to the crystallization of nepheline or plagioclase and is strongly dependent of silica activity and Cl and SO_4 fugacities in the silicate liquid (liq) with the following incongruent reactions (Stormer and Carmichael 1971):

$$Na_4Al_3Si_3O_{12}Cl = NaCl + 3\ NaAlSiO_4 \quad (1)$$

Sodalite liq nepheline

$$Na_4Al_3Si_3O_{12}Cl + 6\ SiO_2 = NaCl + 3\ NaAlSi_3O_8 \quad (2)$$

Sodalite liq liq albite

$$Na_8Al_6Si_6O_{24}(SO_4) + 12\ SiO_2 = NaSO_4 + 6\ NaAlSi_3O_8 \quad (3)$$

Nosean liq liq albite

Xanes and electron microprobe studies from Jugo et al. (2010) and Hettmann et al. (2012), respectively, corroborated the presence of sulfur as pure sulfate (SO_4^{2-}) in haüyne from Eifel, Germany and the high oxidation state at pre-eruptive conditions, whereas nosean in syenite has a large proportion of S^{2-} (e.g. sodalite from Ilimaussaq in Greenland and Mont Saint Hilaire in Canada suggesting more reduced conditions. These previous studies demonstrated that the sulfate/sulfide ratio in sodalite is strongly correlated with oxidation

state of the magmas (Hettmann et al. 2012) and that the determination of S^{6+}/S^{2-} ratio is a powerful tool to estimate the pre-eruptive redox state of alkaline magmas.

The phase equilibrium and conditions of crystallization have been studied experimentally in two natural phonolites (Berndt et al. 2001, Giehl et al. 2014). Haüyne from Laacher See phonolite crystallized at relatively low temperature and pressure (760-840°C, 200-400 MPa) from water-undersaturated melt with 6 wt% H_2O at oxidized conditions at ΔNNO+2.3 (ΔNNO = log$f$$O_2$ - log$f$$O_2$ of the Ni-NiO buffer calculated at P and T) (Berndt et al. 2001), whereas sodalite from Ilimaussaq phonolite crystallized at 650-825°C, 100 MPa, in water-undersaturated and reducing conditions (low H_2O content: 1.2 wt%, ΔNNO-0.5 to ΔNNO-1; Giehl et al. 2014). So far, neither the stability of nosean nor the crystallization of sodalite-group minerals in complex fluid (e.g. with CO_2, S and Cl) has been investigated experimentally.

II. Sodalite-bearing phonolites

II.1. Haüyne-bearing phonolite, Laacher See, Eifel, Germany

Haüynes have been reported in Laacher See phonolitic pyroclastic deposits (N50°24'48", E7°16'24") (Wörner and Schmincke 1984a, Bogaard 1995, Schmincke et al. 1999) from the youngest (12900 ± 560 yr BP) eruptive centers of Quaternary East Eifel volcanic field (400-13 ka). East Eifel volcanic field erupted basanite, leucitite, nephelinite and tephrite with a total magma volume of 1 km^3, whereas the Laacher See volcano erupted about 5 km^3 of phonolitic magma (Bogaard 1983) with alternately plinian and phreatomagmatic phase eruptions of ash, pumice and pyroclastic flows that attest of large volume of dissolved magmatic fluids at depth. The Laacher See tephras (only phonolitic rocks) are divided into 3 units based on stratigraphic position (Wörner and Schmincke 1984a): LLST (Lower Laacher See Tephra, that corresponds to the upper part of the magma chamber), a highly vesicular and

crystal-poor pumice (<5 % phenocrysts of sanidine), MLST (Middle Laacher See Tephra) with 15 vol.% phenocrysts of sanidine, clinopyroxene (cpx), amphibole and biotite, and ULST (Upper Laacher See Tephra, that corresponds to the lower part of the magma chamber) with 50-60 vol.% phenocrysts of sanidine, plagioclase and haüyne. Laacher See phonolites are silica-rich (54.4-58.7 wt% SiO_2) and Mg-poor ($Mg\#=Mg/Mg+Fe^{tot}=0.06-0.15$) (Figure 1). They have higher K_2O content (6.6-8.7 wt%) relative to Na_2O (4.9-7.3 wt% Na_2O; $Na_2O/K_2O=1.2-0.6$) and are slightly peralkaline ($Na+K/Al=0.96-1.08$). Laacher See phonolites have high concentrations in Rare Earth Elem37ents (REE) (80-160 ppm La; 150-200 ppm Ce; 0.5-2.4 ppm Eu, La/Yb=36.5-47.5), Rb (88-188 ppm), Sr (798-1385 ppm) and volatile elements: F (700-1400 ppm), Cl (1200-5500 ppm) and S (300-2000 ppm) (Wörner and Schmincke 1984a). Major, trace element and isotope studies constrained the differentiation of phonolitic magmas to fractional crystallization of olivine, cpx, plagioclase, amphibole, FeTi-oxides and apatite from nepheline basanite and very limited assimilation of crustal rocks (Wörner and Schmincke 1984b; Wedepohl et al. 1994). Sodalite-group minerals have been reported in all LLST, MLST and ULST tephras (Wörner and Schmincke 1984a). They are blue minerals with 0.3 wt% Cl in LLST (rare), MLST (rare) and in ULST (abundant) and white or black (with abundant small sulfide inclusions) minerals with 1-1.5 wt% Cl in LLST and MLST.

II.2. Nosean-bearing phonolite, Saghro, Morocco

Sodalite-bearing phonolites are present in Cenozoic volcanic rocks from the Saghro volcanic field in Anti-Atlas (Morocco) on the northern edge of the West African Craton (9.6-2.9 Ma, Berrahma et al. 1993; Berger et al. 2009). The volcanic deposits are nephelinite lava flows (low volume; 6 km^3, Missenard and Cadoux 2011), phonolitic domes and pyroclastic deposits (Ibhi et al. 2002; Berger et al. 2009). According to the bulk composition and mineral

assemblages, three groups of phonolites have been identified with variable silica content and Mg# (50.0-55.5 wt% and 0.04-0.31, respectively, Figure 1): Sr-rich and alkaline phonolite, peralkaline phonolite, and Si-enriched phonolite (Berger et al. 2009, 2014). All phonolites are depleted in K_2O (5.4-7.7 wt%) relative to Na_2O (5.7-10.6 wt%; Na_2O/K_2O=0.74-1.87) and are peralkaline (Na+K/Al=0.85-1.2). Saghro phonolites have high content in incompatible elements with high REE content (Berger et al. 2014) and are enriched in Light-REE (LREE) compared to Heavy-REE (HREE) (La/Yb=32.3-40.1). Geochemical modeling shows that Si-enriched phonolites are residual melt after fractional crystallization of olivine, cpx, amphibole, magnetite, apatite and alkali feldspar from nephelinitic melt, and crustal assimilation (Figure 1, Berger et al. 2009, 2014).

III. Analytical Methods

Major elements

Whole-rock major elements were measured by wide-angle X-ray fluorescence (WDXRF) using sequential spectrometer Bruker S4 Pioneer at the analytical services of the Instituto Andaluz de Ciencias de la Tierra (IACT, Spain) using Rh X-ray (160 KV, 159 mA). One gram of whole rock powder is weighed with di-lithium tetraborate flux (8:1 flux:rock) and the mixture is fused at 1000°C during 15 minutes. The concentrations of major elements are measured by comparing the X-ray intensity for each element with the intensity for two fused beads each of nine reference geological standard samples.

The concentrations of major elements in minerals were determined using electron microprobe (Cameca XS100 at the 'Microsonde Sud' facility of the University of Montpellier, France). Operating conditions comprised an accelerating voltage of 20 keV, a 10 nA beam current and a beam focalized (1 µm). The counting time was fixed at 20 s for each element analysis and 40s for volatile element (S, Cl). The standards used for major and volatile

element analyses are: wollastonite for Si and Ca, Al_2O_3 for Al, TiO_2 for Ti, forsterite for Mg, hematite for Fe, orthose for K, albite for Na, apatite for P, native metal for Ni, Mn, Cu, baryte for S and Ba, pyrite for S, apatite for F and chloroapatite for Cl.

The valence state of S was determined for haüyne and nosean by measuring the wavelengths of the S Kα X-rays using electron microprobe wavelength-dispersive spectrometry (WDS) and an LPET crystal (Carroll and Rutherford 1988). We counted the S X-rays with a spectrometer sin θ range of 0.61158 - 0.61657 using sin θ steps of 0.00001, a dwell time of 100 ms per step, and a beam of 10 μm. The electron beam was set at 20 keV and 20 nA current, and we accumulated 5 scans for $BaSO_4$ and FeS_2 reference standard analysis, and 10 scans for haüyne and nosean analysis to improve precision.

Whole rock volatile element analyses

Whole rock sulfur and carbon (total carbon and total organic carbon) concentrations were determined for each sample by element analyzer (IACT, Spain, Alt et al. 2012). Total Inorganic Carbon (TIC) and carbonate carbon was removed by reaction with dilute (3 N) HCl, followed by washing in distilled H_2O. To minimize adsorption of atmospheric CO_2, powders were degassed at 100°C and stored under vacuum in a dessicator. Standard deviations were between 10-40 ppm for sulfur and 10 ppm for carbon.

Whole rock F and Cl contents were determined by wet precipitation-ferrithiocyanate spectrophotometry using Varian Cary 50 spectrophotometer at the SARM (Nancy, France). Standard solutions were used to check the accuracy of the analyses. Standard deviations are less than 5% (Vernet et al. 1987).

Trace elements

Whole rock analyses were performed using a quadrupole 7700x inductively coupled plasma mass spectrometry (ICP-MS) at the AETE facility (University of Montpellier, France). 0.1 gram of whole rock powder was dissolved with acid (HF- HNO_3). Blanks were prepared with samples spiked with In and Bi to monitor internal drift. Solutions were analyzed at a final dilution factor of 8000. ICP-MS sensitivity in this configuration was 200.10^6 c.p.s. ppm^{-1} ^{115}In. Analytical accuracy was estimated from measurements of international rock standards UBN and G1.

Trace element concentrations in minerals were determined by a laser ablation ICP-MS system at the University of Montpellier (France), using GeoLas Q + Excimer CompEx102. The diameter laser beam was 26 and 56 μm; a laser repetition rate of 6-10Hz and a laser power of 0.5 mJ (5 J cm^{-1}) were used for this study. The NIST612 standard, USGS standard BIR-1, BHVO-1 and a NiS bead doped with PGE (Platinum group elements) were used as external standard and SiO_2, CaO and S content determined by electron microprobe were used as internal standard. The drift is compensated by the internal standard calculations in the Glitter software (Van Achterbergh et al. 2001); no other drift corrections are used. For data processing and calculation of concentrations, Glitter Software was used to process the raw data files containing the signal intensity versus time. This allows precise selection of blanks and signals, and rapid visualization of the intensity data.

IV. Results

IV.1. Haüyne-bearing phonolite, Laacher See, Eifel, Germany

For this study, we selected the more silica-rich tephra (ULST tephra) containing 5 vol.% of sodalite. This lava is peralkaline (Na+K/Al=1.03) with 58.7 wt% SiO_2 and 8.7 wt% K_2O and plots into the silica-rich group of phonolite in TAS diagram (Figure 1). Our sample has

high concentrations in REE (32.3 ppm La; 56.1 ppm Ce; 0.98 ppm Eu, La/Yb= 47.5), Ba (2052 ppm), Sr (919 ppm) and volatile elements: C (391 ppm), F (440 ppm), Cl (820 ppm) and S (4000 ppm). It contains up to 60 vol.% phenocrysts of cpx (3 vol.%), sanidine (37 vol.%), haüyne (5 vol.%), plagioclase (12.5 vol.%), amphibole (1 vol.%) + magnetite (1 vol.%, $X_{ulvo} = 0.10$), titanite (0.3 vol.%), apatite (0.3 vol.%) and sparse pyrrhotite (Figure 2a).

Sodalite-group mineral occurs as phenocrysts (1 mm in size, 5 vol.%, Figure 2). They are Ca-rich (9.7-9.9 wt% CaO) and Na-poor (15.1-15.4 wt% Na_2O) (Figure 3, Table 2). Sodalites in Laacher See tephra are haüynes according to the classification of Lessing and Grout (1971) (Figure 3). The concentration of S is higher than Cl (5.2 to 5.6 wt% S; 0.3 to 0.5 wt% Cl) and the peak position determined by WDS is very close to the peak position of $BaSO_4$ standard indicating that sulfur in haüyne is predominantly present as S^{6+} (2.3082 keV and 2.3081 keV, respectively, S^{6+}/S^{tot} =0.91 ±0.04, see Hettmann et al. 2012 for method). The sums of oxides from microprobe analysis are close to or higher than 100, suggesting that no or minor CO_2 and H_2O are present in haüynes. Haüynes are enriched in LREE compared to HREE (La/Yb=325-1030) with a strong Eu positive anomaly (0.2-0.28 ppm Eu, $Eu/Eu^*=[2Eu_n]/([Sm_n]+[Gd_n])$=2.1-3.5) and have low concentrations of high field strength elements (HFSE) (e.g. 0.1 ppm Zr, Ta and Hf <0.1 (detection limit)) (Table 2, Figure 4). These minerals have low content in Cu (<1 ppm), Ni (<1 ppm), Re (20-100 ppb), PGE (Pd, Ir) and chalcophile elements (Se, Te) have not been detected (Table 2).

Cpx are unzoned augite phenocrysts (200-800 µm, WoEnFs=49:30:21; Mg#=0.37-0.40) (Figure 2 and Table 2). The REE concentrations display a concave pattern slightly enriched in LREE compared to HREE (La/Yb= 8.9-9.1; Figure 4). Plagioclases are present as phenocrysts (500 µm, An_{46}) and as inclusions (An_{35}) in sanidine. Plagioclases are enriched in LREE compared to HREE (La/Yb= 3200-3400) and have a strong Eu positive anomaly (0.72-0.74 ppm Eu, Eu/Eu*=7.49-12.15) (Figure 4, Table 2). Sanidine phenocrysts (37 vol.%) are K-rich

with $An_4Ab_{28}Or_{68}$ and contain high Ba and Sr content (4200 and 1725 ppm, respectively; Table 3). Rare amphiboles are kaersutite crystals (100 μm), they are Ti-rich (4.6-4.8 wt% TiO_2) and Fe-rich (16.1-16.6 wt% FeO).

Accessory minerals are present as inclusions in cpx and/or in the matrix. Titanites occur as inclusions in cpx. They have very high REE concentrations (4000 ppm La; 10 ppm Lu, Figure 4), Nb (9000 ppm) and Zr (5700 ppm) with small negative Eu anomaly (Figure 4, Table 2). Apatites (50-100 μm) are present as inclusions in cpx and interstitial crystals in the matrix. They are fluoro-apatites (3.26-3.67 wt% F, 0.22-0.25 wt% Cl) and contain up to 0.77-0.95 wt% SO_3. Apatites have high REE content (La/Yb= 60.1 to 93.7, Figure 4), Eu negative anomaly, and low Sr and Ba contents (5 and 0.23 ppm, respectively) (Table 2). Sulfides are scarce and occur as inclusions in magnetite and cpx. Two pyrrhotites (N_{FeS}=0.96) with low Cu content (0.3 wt%) and very low Ni content (0.02 wt%) have been found as inclusions in cpx and magnetite (Cu/Ni=24.6 and 89.4, respectively; Table 3). The concentrations in chalcophile and siderophile elements are variable (i.e. 7-100 ppm As, 10-20 ppm Se, 1-3 ppm Te, 6-40 ppb Ir; Table 3). One single crystal of bornite in cpx has been identified (62 wt% Cu, 25.4 wt% S, 14% wt% Fe, Table 3). Bornite is richer in chalcophile Se (500 ppm) and siderophile (Ir =80 ppb) elements than pyrrhotite. FeTi-oxides in the matrix and as inclusions in cpx are magnetites ($X_{ulvö}$=0.10).

IV.2. Nosean-bearing phonolite, Saghro, Morocco

Sodalite minerals are only present in silica-poor peralkaline phonolites (52.2-54.4 wt% SiO_2, Mg# =0.07-0.31, Na+K/Al = 1.05-1.20 (Figure 1)). We selected a more silica-poor phonolite with 3 vol.% sodalite (Table 1, Figures 1 and 2). This phonolite has lower K_2O content (6.75 wt%) relative to Na_2O content (9.6 wt%; Na_2O/K_2O=1.4) and is peralkaline (Figure 1). Our sample has high concentrations in REE (70.9 ppm La; 108 ppm Ce; 1.4 ppm

Eu, La/Yb= 26.3), Ba (609 ppm), Sr (1146 ppm). The concentrations of volatile elements are high for Cl (2530 ppm) and low for C (130 ppm), F (520 ppm), and S (560 ppm) (Table 1).

The investigated phonolite is crystal-poor (12 vol.% phenocrysts) with cpx (1.5 vol.%), sanidine (3.5 vol.%), nepheline (6 vol.%), nosean (0.4 vol.%), altered amphibole (0.1 vol.%), magnetite (0.3 vol.%), titanite (0.05 vol.%), apatite (0.05 vol.%) and pyrrhotite (<0.01 vol.%). Sodalite minerals (1 mm, grey-brown colour, Figure 2) have high Na_2O and K_2O content (18-23 and 0.5-3.3 wt%, respectively; Figure 3a), high S and low Cl content (S= 2.8 to 3.5 wt%; Cl=0.75-1.27 wt%; Figure 3b), and S > Cl, characteristic for nosean (Na-S-Cl sodalite) (Lessing and Grout 1971). λ(S Ka) peak position for Saghro nosean is between S^{6+} ($BaSO_4$) and S^{2-} (FeS_2) indicating that both sulfur species, S^{6+} and S^{2-}, are present (λ(S Ka) = 2.30805 keV, S^{6+}/S^{tot}=0.87±0.04; see Hettmann et al. 2012 for method). Noseans have high LREE content (3-10 ppm La), low Middle-REE (MREE) (0.2-0.3 ppm Sm) and HFSE (1.4-6 ppm Zr, <0.1 ppm Hf) contents, very low HREE content (<0.01 ppm) and a strong Eu negative anomaly (Figure 5b). Noseans have variable Cu (6-500 ppm) and Ni (0.5-23 ppm) contents and, siderophile element contents (Pd, Ir). Although sulfide-free crystal surfaces have been analyzed, high Cu content may be due to the presence of tiny sulfide crystals at depth. Chalcophile elements (Se, Te) have not been detected (Table 4). Nosean crystals have reaction rims (150-200 µm, Figure 2) with low Na_2O (15 wt%) and high K_2O and FeO content (10 wt% and 3 wt%, respectively). Cl content is lower (0.06 wt%) at the rim than at the core, whereas S content is constant (3-2.5 wt% S) (Figure 3b).

Cpx are phenocrysts (300 µm) with green core and yellow rim. The cores are rich in MgO (Mg#=0.7-0.8), Al_2O_3 (8-10 wt%), TiO_2 (3-4.5 wt%), and Cr_2O_3 (0.15-0.3 wt%). REE patterns show a concave shape enriched in LREE compared to HREE (20-30 ppm La, 8-10 ppm Sm, 0.1-0.5 ppm Lu, Figure 5a, Table 3). Trace element analyses display relatively high content of Zr (300-400 ppm), Rb (0.02-3.7 ppm), and Sr (60-650 ppm). There is an abrupt

change in composition at the rim of cpx crystals. The rims are 100 μm wide and have low MgO (Mg#=0.4-0.6), and high FeO (11-13.7 wt%) and Na_2O (2.5-3 wt%) content. The rims are enriched in Zr (400-2700 ppm), LREE (30-100ppm La) and HREE (0.25-1.6 ppm Lu) and depleted in MREE (6-7 ppm Sm) compared to the core (Figure 5a, Table 3).

Nepheline crystals are euhedral (1 mm) with high Na_2O (11.2-13.25 wt%) and SiO_2 content (43.3-48.5 wt%) (Table 2). The concentrations of trace elements in nephelines are below the detection limit for trace elements, except for Rb, Sr and Ba (82, 42, 7.4 ppm, respectively). Rare sanidine crystals (<100 μm) have less than 0.01 wt% CaO and Or_{73}.

Titanites are euhedral crystals (300 μm) in the matrix with high LREE content (La/Sm=6.6-7.7, La/Yb= 49-51) (Figure 5, Table 2). Apatites are fluoro-apatite microcrystals (20-30μm in size) with no S and Cl (up to 3 wt% F, <0.04 wt% Cl, and 0.05-0.1 wt% SO_3 (200-400 ppm S)). Apatites as inclusion in cpx and titanite have high REE concentrations (2800-3200 ppm La; 2.1-3.4 ppm Lu) and Sr (9800-13000 ppm) and low Cu/Ni ratio (0.29-0.65). Interstitial apatites have higher Sr content (10000-18000 ppm) and Cu/Ni ratio (1.2-1.4) relative to the apatite as inclusions in cpx (9000-12000 ppm Sr) and titanite. Sulfides are relatively abundant and have pyrrhotite composition ($Fe_{1-x}S$) with low Cu and Ni content (<2 and <1.4 wt%, respectively; Cu/Ni=0.05-50, Table 4). Pyrrhotites as inclusions in cpx have N_{FeS} values from 0.90 to 0.92, whereas interstitial pyrrhotites have higher N_{FeS} values (0.92-0.98). The concentrations of chalcophile elements are variable (6-1000 ppm As, 10-150 ppm Se, 0.4-5 ppm Te) and the concentrations of siderophile elements are very low (i.e. I-PGE (Os, Ir, Ru) are often under detection limit (Table 4)). FeTi-oxides are interstitial magnetites with Xulvö=0.15-1.16 and 0.03-0.10 wt% Ni and 0.01 - 0.05 wt% Cu (Cu/Ni =0.1). Table2

V. Discussion

V.1. Crystallization of sodalite minerals

The stability of pure sodalite ($Na_8(AlSiO_4)_6(Cl_2, SO_4)$) is directly related to incongruent reaction of melt with nepheline and albite (reactions 1 and 2 above, Stormer and Carmichael 1971). However, the presence of Ca in natural sodalite and feldspar (Figure 3, Table 2) requires both Na and Ca in the equilibrium reactions to constrain the solid solution for sodalite-group minerals and determine the stability of sodalite and feldspar in natural systems. Using mineral stoichiometry (Table 2) and phase equilibria in phonolites, we established the reaction for haüyne (Ca-bearing sodalite) and plagioclase in Laacher See phonolite and nosean (Ca-free sodalite) and nepheline in Saghro phonolite.

For Ca-bearing minerals (Laacher See phonolite), the reaction can be expressed as follows:

$$Na_{4.5}Ca_{1.5}Al_6Si_6O_{24}(SO_4)_2 + 4\ SiO_2 + 1.5\ Na_2O + 0.25\ O_2 = 4\ Na_{0.25}Ca_{0.4}(Al_{1.4}Si_{2.6})O_8 + 2\ Na_2SO_4$$

Haüyne liq liq plagioclase liq (4)

The presence of silica and sodium (component in the melt) on the left side of the incongruent reaction (4) indicates that low silica and low sodium activity would promote the crystallization of haüyne (feldspathoid), whereas plagioclase crystallized from silica-saturated silicate melt. Since oxygen is also present on the left side of the equation it indicates that the reaction from haüyne to plagioclase consumed oxygen, and the silicate liquid becomes more oxidized as plagioclase crystallized.

For Ca-free sodalite, in Si-undersaturated silicate liquid with low silica activity and low volatile activity, nepheline is the first phase to crystallize leading to an enrichment of silica and volatile (Cl and SO_4^{2-}) in the residual melt (Barker 1976; Sharp et al. 1989). This continues until nosean begins to crystallize. NaCl and Na_2SO_4 activity of the magma is then buffered as follows:

403 $6\ NaAlSiO_4 + 1.5\ Na_2SO_4 + 0.75\ NaCl + 3.4\ O_2 = Na_8Al_6Si_6O_{24}((SO_4)_{1.5}, Cl_{0.5}) + 1.5\ Na_2O$

404 nepheline liq liq nosean liq (5)

405 The incongruent reaction nepheline/nosean constrains the crystallization at high Na_2O
406 activity. Again, the reaction consumed oxygen as nosean crystallizes. Consequently, for both
407 cases, the oxygen fugacity increases and the magma becomes more oxidized.

408 Haüyne and nosean have similar REE patterns, enriched in LREE compare to MREE
409 (La/Sm=35.4-46.4 and 20.2-36.5 for haüyne and nosean, respectively, Figures 5 and 6). The
410 strong positive Eu anomaly, present only in haüyne crystal (Figure 5b), suggests that Eu
411 substitutes to cation in the structure of haüyne ($Kd_{mineral/matrix}$ (in situ) varies from incompatible
412 (Kd=0.05, Francalanci et al. 1987) to moderately incompatible (Kd=0.6, Wörner et al. 1983)).
413 The element distribution in haüyne is thus very similar to what is observed in plagioclase
414 (Figure 4) with Eu^{2+}-Ca^{2+} substitution (Schnetzler and Philpotts 1970).

415 In nosean (Ca-free), Eu should behave as incompatible elements with Eu^{3+} behaving like
416 Sm and Gd (no Eu anomaly). The strong negative Eu anomaly observed in nosean (Figure 5)
417 is then related to prior crystallization of Eu^{2+}-rich minerals and to Eu-depleted composition of
418 the silicate melt from which they crystallized. The absence of plagioclase and the absence of a
419 negative Eu anomaly in cpx, titanite and apatite, however, suggest that the Eu anomaly in
420 nosean is not related to the crystallization of Eu-bearing minerals. The negative anomaly can
421 then be the consequence of a very low Eu^{3+}/Eu^{2+} ratio in parental silicate melt, which makes
422 Eu more incompatible than neighboring REE. Similar negative anomalies have been
423 previously observed in zircon and were related to the oxidation state of the magma (Trail et al.
424 2012). Drake (1975) estimated from Eu and Sr partitioning in plagioclase that Eu^{3+}/Eu_{total} =
425 0.5 at ΔNNO-3 and recent experimental data by Cicconi et al. (2012) suggest a strong control
426 of the silicate melt composition on Eu speciation (Eu^{3+}-Eu^{2+}) (Eu^{3+}/Eu_{total} = 0.5 at ΔNNO-1
427 for haplogranitic melt). Considering that nosean contains sulfur as sulfide (S^{2-}) and sulfate

(S^{6+}), we can, however, infer that the crystallization environment of phonolitic melt was oxidized, close to NNO (Jugo et al. 2010) and the silicate melt contains predominantly Eu^{2+}. Thus, the change of Eu speciation from Eu^{2+} to Eu^{3+} may occur at high oxygen fugacity in alkaline undersaturated silicate melt and the Eu anomalies in nosean represent a potential oxygen fugacity barometer, which could be calibrated experimentally.

V.2. Pre-eruptive conditions of sodalite-bearing phonolitic magma

The pre-eruptive conditions (temperature (T), pressure (P), fugacities of volatiles) of phonolitic magma can be constrained using the mineral assemblage present in the rock and the composition of minerals (major, minor, volatile and trace elements). The depth and temperature of crystallization can be estimated assuming equilibrium between cpx and silicate melt and using the composition of both phases (Masotta et al. 2013; Putirka et al. 2003; Putirka, 2008; Mollo and Masotta 2014). In Laacher See and Saghro phonolites, the silicate melt in equilibrium with cpx has been calculated using trace element concentrations in cpx and published partition coefficient using matrix mineral compositions from stratified layer ULST (sample 1088, Wörner et al. 1983). The composition of silicate melts calculated from cpx composition is very close to the measured bulk rock composition (Figures 7 and 8), suggesting that cpx are suitable as thermobarometer. The thermobarometer defined by Masotta et al. (2013) for alkaline differentiated magmas (σT=15°C - σP=115 MPa) constrains the equilibrium pressure at 220-270 MPa and 760-870°C for Si-rich phonolite (Laacher See) and 280-330 MPa and 925-950 °C for Si-poor phonolite (Saghro) (Figure 6). Using the method of Mollo and Masotta (2014) to minimize the error of temperature (e.g. considering the difference between predicted and observed components in cpx, ΔDiHd=0.02), the equilibrium temperature for Laacher See is the highest estimated temperature with T=850°C (P=250 MPa) for Laacher see and T=950°C (P=300 MPa) for Saghro phonolites (Figure 6).

453 The relatively high temperature and low pressure of Laacher See phonolite agree with
454 previous estimates from mineral compositions and xenolith evidence (Wörner & Schmincke,
455 1984b) and with experimentally determined pre-eruptive conditions for the ULST Unit of
456 Laacher See, i.e. 200 MPa and 830-870°C (Berndt et al. 2001). The higher crystallization
457 temperature of nosean-bearing phonolite (Cl-rich) is consistent with the higher temperature of
458 crystallization of Cl-sodalite determined experimentally relative to SO_4-sodalite (Tomisaka
459 and Eugster 1968).
460
461 The fugacities of volatile elements (i.e. fO_2, fS_2) represent the redox state of the magmatic
462 system and controlled the crystallization and the composition of minerals and the phase
463 equilibria. The fugacity of oxygen may be estimated using phase assemblage, mineral
464 composition and element speciations in mineral and melt. The oxygen fugacity strongly
465 controlled the speciation of iron (Fe^{3+}/Fe^{2+}) and sulfur (S^{6+}/S^{2-}) in the silicate melt and the
466 crystallization of ferrous/ferric mineral and sulphate/sulphide mineral (i.e. Carroll and
467 Rutherford 1988; Jugo 2009). In phonolite, the co-crystallization of sulfate-bearing sodalite
468 (S^{6+}) and apatite (S^{6+}) as well as sulphide (S^{2-}) in both nosean and haüyne-bearing phonolite
469 indicates that the redox state of phonolitic magmas at pre-eruptive conditions was relatively
470 oxidized with an oxygen fugacity close to ΔNNO-NNO+1 (Jugo 2009; Jugo et al. 2010).
471 Pyrrhotite is present in silicic magmas at reduced and intermediate oxidation state (i.e.
472 ΔNNO-NNO+1) (e.g. Carroll and Rutherford 1988; Luhr 1990; Clemente et al. 2004; Parat et
473 al. 2008) and the composition (N_{FeS}) is function of the sulfur fugacity of the silicate melt and
474 the temperature (Toulmin and Barton 1964; Whitney 1984). In the Laacher See phonolite, rare
475 pyrrhotites as inclusions in cpx and magnetite indicate that they crystallized close to the
476 liquidus and their composition (low N_{FeS}, Table 4) is representative of the liquidus
477 environment (Whitney 1984). Assuming that both cpx and pyrrhotite are liquidus phases and

considering the temperature of crystallization of cpx (T=850°C), the sulfur fugacity estimated from pyrrhotite composition (N_{FeS}= 0.92-0.93) is logf_{S2} = 0.02 to -0.69 (1-0.2 bar). For Saghro phonolite, pyrrhotites have low S content and N_{FeS}= 0.92-0.97. For T=950 °C, logf_{S2} = 0.8 to -2.3 (7 to <0.1 bar). The coexistence of magnetite ($X_{ulvospinel}$ = 0.08-0.17) and pyrrhotite at 850 and 950°C indicates an oxygen fugacity close to ΔNNO-NNO+1 for Laacher See phonolite and ΔNNO-0.7-ΔNNO+1 for Saghro phonolite (Whitney 1984), in agreement with sulphate/sulphide crystallization (Jugo 2009) and high-Cl content in sodalite minerals (Stormer and Carmichael 1971).

V.3. Volatile element concentrations and speciation in phonolitic melt

The abundance of volatile elements CO_2, H_2O, S and halogens dissolved in magmas are strongly variable because their solubility and ability to be fractionated in minerals and in the vapor phase depend on several parameters such as pressure, temperature, melt composition and redox state. In phonolitic melts, water, CO_2, and S partition less strongly in favor of fluids, by an order of magnitude, compared to rhyolitic or dacitic melts owing to greater solubilities of these volatiles in the melt (Scaillet & Pichavant 2003; Webster et al. 2011, 2014). Also, the partitioning of Cl, H_2O, CO_2 and F varies with the molar ratio (Na_2O/Na_2O+K_2O) of the melts (Webster et al. 2014). The two phonolitic system studied here show a strong variability of volatile according to mineral assemblage and composition that may be related to their different alkalinity and/or initial volatile content in parent nephelinite (Saghro) and nepheline basanite (Laacher See).

H_2O and CO_2 content in phonolites

H_2O and CO_2 are the most abundant volatile elements in magmatic systems (e.g. Johnson et al. 1994; Métrich and Wallace 2008). In phonolitic magmas, the H_2O content are highly

503 variable from 1 to 5 wt% H_2O and CO_2 can reach up to 3000 ppm (e.g. Signorelli et al. 1999;
504 Scaillet et al. 2008, Oppenheimer et al. 2011). The hygrometer from Mollo et al. (2015),
505 specific for phonolitic-trachytic melt, allows us to estimate the water content in Laacher See
506 silicate melt in equilibrium with sanidine at 5.9 (±0.7) wt% H_2O suggesting that minerals
507 have crystallized close to water-saturated conditions (Schmidt and Behrens 2008; Webster et
508 al. 2014). This value corroborates data from melt inclusions (<6 wt% H_2O, Harms and
509 Schmincke 2000) and experimental study at 200 MPa and water-saturated and CO_2-free
510 conditions (Berndt et al. 2001). The presence of CO_2, S and, Cl lowered the water solubility in
511 phonolitic melt (at 900°C, H_2O solubility is 6.5 and 8 wt% in Cl-bearing and CO_2-free
512 phonolitic melt and in Cl-CO_2-free phonolitic melt, respectively, Webster et al. 2014) leading
513 to the presence of a fluid phase at depth. However, for Laacher See, the low bulk CO_2 content
514 in phonolite and CO_2-free melt inclusions reported by Harms and Schmincke (2000) suggest
515 that CO_2 was not a factor that may have induced fluid saturation in the phonolitic magma.
516 Contrary to Laacher see phonolite, Saghro phonolite has not been studied experimentally
517 and does not have melt inclusions in phenocrysts or glassy matrix. The bulk CO_2 content
518 suggests a minimum value of 130 ppm C after degassing (Table 2), whereas the water content
519 can only be estimated using K-feldspar-melt equilibrium (Mollo et al. 2015). Calculation
520 yields water content in the melt coexisting with sanidine equals to 4.1 (±0.7) wt% H_2O. The
521 partitioning of H_2O and CO_2 into the fluid phase increases (and Cl decreases) with increasing
522 molar Na/Na+K in melts (Webster et al. 2014). The lower Na/Na+K ratio of Laacher See
523 phonolite (Na/Na+K=0.48) compared to the Saghro phonolite (Na/Na+K=0.68) as well as the
524 presence of other volatile species indicate water undersaturated conditions for Laacher See at
525 low pressure, whereas Saghro phonolite might have been closer to water-saturated conditions.
526
527 **S content and speciation in phonolites**

The presence of sulfur in phonolitic magmas is clearly demonstrated by the crystallization of S-bearing phases such as pyrrhotite, haüyne, nosean, and S-bearing apatite. Laacher See phonolite has abundant haüyne (5 vol.%, 5.2-5.5 wt% S) and S-rich apatite (0.5 vol.%, 0.7-0.9 wt% SO_3), whereas pyrrhotites are rare and the whole rock sulfur content of the phonolite after eruption (i.e. minerals and silicate melt after volatile exsolution during ascent) is high with 4000 ppm S.

The initial sulfur content at pre-eruptive conditions can be estimated using experimentally determined partition coefficient for apatite ($Kd_S^{ap/melt}$, Parat et al. 2005, 2011). S-rich apatites from Laacher See are in equilibrium with S-rich melt with 1100-3200 ppm S (as S^{6+})**.** These concentrations are higher than those measured in melt inclusions (S=520-1490 ppm) and matrix glasses (S=200-940 ppm) from ULST tephra (Harms and Schmincke 2000), suggesting partial degassing or crystallization of S-bearing mineral phases before melt inclusion entrapment. These values are lower than the whole rock sulfur content suggesting that slight haüyne accumulation may have occurred in the lower part of the magma chamber.

Nosean-bearing phonolites from Saghro have 0.4 vol.% nosean (2.8-3.5 wt% S), relatively abundant pyrrhotite and low whole rock sulfur content (S=560 ppm, Table 2, Figure 9). Apatites are S-poor (SO_3 <0.1 wt%) and the sulfate content (S^{6+}) in the melt in equilibrium with apatite is less than 20 ppm. Nosean-bearing phonolites from Saghro are sulfate-poor with low S^{6+}/S^{2-} ratios in the silicate melt (presence of pyrrhotite (S^{2-})).

Cl content in phonolites

Laacher See phonolite has Cl-poor haüyne (0.3-0.5 wt% Cl) and Cl-rich apatite (0.22-0.25 wt% Cl), whereas Saghro phonolite has Cl-rich nosean (1.1-1.3 wt% Cl) and Cl-poor apatite (<0.03 wt% Cl). Cl is present in large amount in Laacher See melt inclusions (1770-2600 ppm Cl) and matrix glasses (2100-5540 ppm Cl) (Harms and Schmincke 2000) relative

553 to bulk rock (820 ppm Cl) (Figure 9). Using experimentally determined partition coefficient,
554 $Kd_{Cl}^{ap/melt}$ for hydrous phonolitic melts (Webster et al. 2009), the Cl concentration in the melt
555 in equilibrium with apatite is 2000-2300 ppm Cl. This is one order of magnitude higher than
556 the concentration estimated for Saghro phonolite, where Cl-poor apatite crystallized from a
557 melt with Cl_{melt} <91 ppm.

558 The Cl solubility in hydrous trachytic and phonolitic melts is strongly dependent of
559 pressure and peralkaline index (Signorelli and Carroll 2002) and decreases with increasing
560 sulfur content (Webster et al. 2014). The two studied phonolites have very different
561 peralkalinity and thus theoretical solubility: for Laacher See phonolite (P=200 MPa,
562 Na+K/Al=1.04), Cl solubility is 5000 ppm, whereas for Saghro phonolite (P=300 MPa,
563 Na+K/Al=1.2) Cl solubility is 8000 ppm (Signorelli and Carroll 2002). The maximum of Cl
564 solubility decreases with S, from 9400 to 6700 ppm Cl in S-poor and S-bearing phonolite,
565 respectively (Webster et al. 2014). These values are higher than those estimated from apatite
566 compositions suggesting that the phonolitic melt was not saturated in Cl during apatite
567 crystallization and the co-crystallization of haüyne in Laacher See phonolite occurs in the
568 absence of an exsolved Cl-bearing fluid (before Cl saturation) (Figure 9). The late
569 crystallization of nosean in Saghro phonolite (Figure 10) may suggest crystallization close to
570 or at Cl saturation in the silicate melt.

571

572 **F content in phonolites**

573 Fluorine is the volatile element that has the lowest partition coefficient between fluid
574 phase and silicate melt (e.g. Webster et al. 2014) and F is mainly incorporated in apatite
575 during fractional crystallization. The partition coefficient of F between apatite and melt has
576 been quantified experimentally and in situ for silicate melt, increasing from basalt to
577 phonolite from 3.4 to 40, respectively (Mathez et al. 2005, Webster et al. 2009; Parat et al.

2011). In Laacher See and Saghro phonolites, the fluorine content in apatite ranges from 3.3 to 3.9 wt%, and using partition coefficient for phonolitic melt, F concentration in the melt in equilibrium with apatite is 800-1000 ppm. These values are lower than the concentration of F solubility determined experimentally for phonolitic melt (5000-7500 ppm, Webster et al. 2014) suggesting that at the time of apatite crystallization, the silicate melt was undersaturated in F.

V.4. Crystallization environment of sodalite-bearing phonolites

Haüyne-bearing Si-rich phonolite - Laacher See

The Laacher See phonolite represents a late stage of crystallization that evolved from nepheline basanite magmas (Wedepohl et al. 1994, Wörner and Schmincke 1984b). The phonolitic magma is Si-undersaturated and peralkaline and the crystallization of cpx, plagioclase, amphibole, apatite, haüyne, sanidine, pyrrhotite, magnetite occurs at depth in a shallow magma chamber (250 MPa and 850°C). The crystallization environment is oxidized (ΔNNO-NNO+1) and the oxidation state increased with crystallization (haüyne-plagioclase crystallization). More oxidizing conditions at the top of the Laacher See magma chamber are also indicated by the speciation of sulfur in glass inclusions, the S^{6+}/S^{tot} ratio being higher in the LLST (top of the magma chamber) than in the ULST (bottom of the magma chamber) (Harms and Schmincke 2000).

The REE compositions of the theoretical silicate melts in equilibrium with cpx, apatite, haüyne, titanite and plagioclase calculated from mineral composition and available empirical partition coefficient for phonolitic system (Wörner et al. 1983; Francalanci et al. 1987; Lemarchand et al. 1987; Villemant 1988; Olin and Wolff 2012; Figures 7 and 8) suggest that minerals have crystallized from a melt with a composition close to the bulk composition. Melt calculated from cpx shows a small discrepancy with a concave shape compare to the bulk

603 rock with a depletion in MREE relative to LREE and HREE suggesting a slightly early
604 crystallization of titanite before cpx crystallization (Kd(titanite/melt) for MREE = 38-72 in
605 titanite, Olin and Wolff 2012) in agreement with the occurrence of titanite as inclusions in
606 cpx. The rims of cpx are depleted in MREE and enriched in HREE compared to the core
607 (Figure 5), suggesting that titanite also crystallized during the crystallization of cpx rim. The
608 trace element concentrations with different compatibility such as Cu/Ni (Cu is incompatible in
609 silicate minerals, whereas Ni is moderately compatible; Ewart and Griffin (1994)) corroborate
610 one crystallization environment for all minerals with similar Cu/Ni ratio (Figure 10). The
611 coeval crystallization of minerals in Laacher See phonolite agrees with the study of Harms
612 and Schmincke (2000) in which melt inclusions in all minerals from the ULST have very
613 similar composition (57-59 wt% SiO_2).

614 The incongruent reaction haüyne-plagioclase and the negative Eu anomaly observed in
615 cpx, titanite and apatite, suggest an early crystallization of haüyne leading to an increase of
616 the oxygen fugacity (e.g. magma becomes more oxidized) with differentiation in agreement
617 with experimental and melt inclusion studies suggesting more oxidizing conditions at the top
618 of the Laacher See magma chamber (more evolved magma, LLST; Berndt et al. 2001; Harms
619 and Schmincke 2000). The sequence of crystallization may be then defined as: early
620 crystallization of haüyne-apatite-titanite followed by cpx-plagioclase-sanidine±amphibole.
621 The lower trace element contents and positive Eu anomaly of the studied bulk-rock sample
622 compared to published bulk-rock compositions of Laacher See tephra of the ULST unit and
623 the Eu negative anomaly (Figure 7, Wörner et al. 1983; Wörner and Schmincke 1984a)
624 indicate, as discussed for volatile elements, that accumulation of haüyne and possibly
625 plagioclase may have occurred in the lower part of the magma chamber.

626 During crystallization, the water content in the phonolitic melt (<6 wt% H_2O) indicates
627 that at depth (250 MPa), the melt was fluid-undersaturated. However, the evolution of S, Cl,

628 and F content in the melt in equilibrium with apatite and in the melt inclusions show an
629 increase of F and constant S and Cl (Figure 9), S being probably buffered by the
630 crystallization of S-rich haüyne, whereas the melt become Cl saturated with differentiation
631 leading to the presence of a NaCl fluid phase (Dalou et al. 2015). More likely the upper part
632 of the magma chamber was water-saturated and the Cl partitioned into an exsolving H_2O fluid
633 phase.
634
635 ***Nosean-bearing Si-poor phonolite – Saghro***

636 The last stage of crystallization of Saghro phonolite represents a moderately peralkaline
637 melt with low silica and low Na_2O activities and the crystallization of nepheline, cpx,
638 sanidine, nosean, apatite and pyrrhotite at high temperature (950°C), low pressure (300 MPa)
639 and relatively oxidized conditions (ΔNNO) in a volatile-poor fluid-undersaturated magma (4
640 wt% H_2O).

641 The trace element ratios and the calculated melt compositions in equilibrium with cpx
642 (Cu/Ni=0.1) and apatite (Cu/Ni=0.3-1.4) suggest that both are early crystallizing mineral in
643 equilibrium with the bulk rock composition (Figures 7a-d and 10). Although the calculated
644 melts are slightly different compared to the bulk rock composition, the uncertainty of the
645 partition coefficient allows us to consider that all minerals crystallized in one environment
646 (Figure 8). The large variability of the Cu/Ni ratio in minerals (Figure 10) suggests however
647 that the evolution of Saghro lava most probably involved a more fractionated differentiation
648 compared to Laacher See. With decreasing temperature, the sequence of crystallization is cpx-
649 nepheline-apatite-pyrrhotite followed by nosean-titanite. The incongruent reaction nepheline-
650 nosean consumed oxygen during nosean crystallization and consequently, the oxygen fugacity
651 increased and the magma became more oxidized.

The volatile content in Saghro phonolitic melt is very low (Figure 9) although it allows saturation of K-rich and Na-poor nosean (S and Cl-bearing) in the late stage of crystallization. The rim of nosean have S content identical to the core, whereas Cl and Na strongly decreases suggesting that during ascent Cl most probably exsolved and formed a NaCl-bearing fluid phase (Figure 3).

Implications

Our work shows that haüyne- and nosean-bearing phonolites are last equilibrated at low pressure and relatively high temperature with different volatile concentrations. Fractional crystallization of olivine+cpx+amphibole+plagioclase+FeTi-oxides+apatite in Laacher See and olivine+cpx+amphibole+magnetite+apatite+alkali feldspar in Saghro from basanite/nephelinite magmas may have led to volatile-bearing silicic peralkaline magmas. The difference in major element composition, e.g. Na, K, and Si and the concentration of volatile elements in Si-rich and Si-poor phonolites are the result of slightly different parental magma compositions and different fractional crystallization evolution involving haüyne or nosean crystallization.

Although fractional crystallization appears to be the main proposed processus for phonolite genesis (e.g. Edgar 1987; Ablay et al. 1998; Thompson et al. 2001), recent experimental study from Laporte et al. (2014) on partial melting of K_2O-bearing lherzolite reproduced the major element composition of nosean-bearing phonolite for very low partial melting. The experiments fail however to reproduce the high SiO_2 and K_2O values in haüyne-bearing phonolite, even for very low partial melting. These experiments are volatile-free and the influence of volatiles in mantle rocks on partial melting should be addressed to constrain the genesis of Si-rich and volatile-rich sodalite-bearing phonolite and other volatile-bearing phonolites (e.g. Signorelli et al. 1999; Oppenheimer et al. 2011) and confirm the hypotheses

677 in which volatile-rich and Si-rich phonolites are the last stage of fractional crystallization of
678 nepheline basanite magmas, whereas volatile-bearing and Si-poor phonolites may result from
679 partial melting of K_2O-rich mantle rocks.
680
681
682 **Acknowledgment**

683 This research was financially supported by the "Institut National des Sciences de
684 l'Univers" (France) (projet 772372). We would like to thank F. Holtz for providing rock
685 samples from Eifel, C. Nevado and D. Delmas for their valuable technical assistance, and J.-
686 M. Dautria for informative discussions. Constructive reviews by G. Wörner and an
687 anonymous reviewer are gratefully acknowledged. We thank C. Cannatelli for editorial
688 handling of the manuscript.
689
690 **References**

691 Ablay, G.J., Carroll, M.R., Palmer, M.R., Marti, J., and Sparks, R.S.J. (1998) Basanite-Phonolite
692 lineages of the Teide-Pico Viejo Volcanic Complex, Tenerife, Canary Islands. Journal of
693 Petrology, 39(5), 905–936.
694 Alt, J.C., Garrido, C.J., Shanks III, W.C., Turchyn, A., Padrón-Navarta, J.A., Sánchez-Vizcaíno,
695 V.L., Gómez Pugnaire, M.T., and Marchesi, C. (2012) Recycling of Water, Carbon, and
696 Sulfur During Subduction of Serpentinites: A Stable Isotope Study of Cerro Del Almirez,
697 Spain. Earth and Planetary Science Letters, 327–28, 50–60.
698 Bailey, D.K. (1987) Mantle metasomatism-perspective and prospect. Geological Society, London,
699 Special Publications, 30, 1–13.
700 Barker, D.S. (1976) Phase Relations in the System $NaAlSiO_4$-SiO_2-NaCl-H_2O at 400°C-800°C and
701 1 Kilobar, and Petrologic Implications. The journal of Geology, 84, 97–106.

Bellatreccia, F., Della Ventura, G., Picciniti, M., Cavallo, A., and Brilli, M. (2009) H_2O and CO_2 in minerals of the haüyne-sodalite group: an FTIR spectroscopy study. Mineralogical Magazine, 73(3), 399–413.

Berger, J., Ennih, N., Mercier, J.-C., Liégeois, J.-P., and Demaiffe, D., (2009) The role of fractional crystallization and late-stage peralkaline melt segregation in the mineralogical evolution of Cenozoic nephelinites/phonolites from Saghro (SE Morocco). Mineralogical Magazine, 73(1), 59–82.

Berger, J., Ennih, N., and Liégeois, J.-P. (2014) Extreme Trace Elements Fractionation in Cenozoic Nephelinites and Phonolites from the Moroccan Anti-Atlas (Eastern Saghro). Lithos 210–11, 69–88.

Berndt, J., Holtz, F., and Koepke, J. (2001) Experimental constraints on storage conditions in the chemically zoned phonolitic magma chamber of the Laacher See volcano. Contributions to Mineralogy and Petrology, 140, 469–486.

Berrahma, M., Delaloye, M., Faure-Muret, A., and Rachdi, H.E.N. (1993) Premières données géochronologiques sur le volcanisme alcalin du Jbel Saghro, Anti-Atlas, Maroc. Journal of African Earth Sciences, 17, 333–341.

Bogaard, V.D.P. (1983) Die Eruption Des Laacher See Vulkans. Ph.D. thesis, Ruhr-Universitat Bochum.

Bogaard, V.D.P. (1995) 40Ar/39Ar ages of sanidine phenocrysts from Laacher See Tephra (12,900 yr BP): Chronostratigraphic and petrological significance. Earth and Planetary Science Letters, 133, 163–174.

Brousse, R., Bizouard, H., and Varet. J. (1969) Iron in the mineraIs of the Sodalite Group. Contributions to Mineralogy and Petrology, 22, 164–84.

Bryan, S.E. (2006) Petrology and Geochemistry of the Quaternary Caldera-forming, Phonolitic Granadilla Eruption, Tenerife (Canary Islands). Journal of Petrology, 47(8), 1557–1589.

Carroll, M.R., and Rutherford, M.J. (1988) Sulfur speciation in hydrous experimental glasses of varying oxidation state; results from measured wavelenght shifts of sulfur X-rays. American Mineralogist, 73, 845–849.

Cicconi, M.R., Giuli, G., Paris, E., Ertel-Ingrisch, W., Ulmer, P., and Dingwell, D.B. (2012) Europium oxidation state and local structure in silicate glasses. American Mineralogist, 97, 918–929.

Clemente, B., Scaillet, B., and Pichavant, M. (2004) The solubility of Sulphur in Hydrous Rhyolitic Melts. Journal of Petrology, 45(11), 2171–2196.

Dalou, C., Mysen, B.O., and Foustoukos, D. (2015) In-situ measurements of fluorine and chlorine speciation and partitioning between melts and aqueous fluids in the Na_2O-Al_2O_3-SiO_2-H_2O system. American Mineralogist, 100, 47–58.

De Fino, M., La Volpe, I., Peccerillo, A., Piccarreta, G., and Poli. G. (1986) Petrogenesis of Monte Vulture Volcano (Italy): Inferences from Mineral Chemistry, Major and Trace Element Data. Contributions to Mineralogy and Petrology, 92, 135–45.

Drake, M.J. (1975) The oxidation state of europium as an indicator of oxygen fugacity. Geochimica et Cosmochimica Acta, 39, 55–64.

Edgar, A.D. (1987) The Genesis of Alkaline Magmas with Emphasis on Their Source Regions: Inferences from Experimental Studies. Geological Society, London, Special Publications, 30, 29–52.

Ewart, A., and Griffin, W.L. (1994) Application of Proton-Microprobe Data to Trace-Element portioning in Volcanics Rocks. Chemical Geology, 117, 251–284.

Francalanci, L., Peccerillo, A., and Poli, G. (1987) Partition coefficients for minerals potassium - alkaline rocks: Data from Roman province (Central in Italy). Geochemical Journal, 21, 1–10.

Fujimaki, H., Tatsumoto, M., and Aoki, K. (1984) Partition coefficients of Hf, Zr, REE between phenocrysts and groundmass. Journal of Geophysical Research, 89, 662–672.

752 Giehl, C., M. Marks, and Nowak. M. (2014) An Experimental Study on the Influence of Fluorine
753 and Chlorine on Phase Relations in Peralkaline Phonolitic Melts. Contributions to Mineralogy
754 and Petrology, 167:977.
755 Harms, E., and Schmincke, H.-U. (2000) Volatile composition of the phonolitic Laacher See
756 magma (12,900 yr BP): implications for syn-eruptive degassing of S, F, Cl and H2O.
757 Contributions to Mineralogy and Petrology, 138, 84–98.
758 Hettmann, K., Wenzel, T., Marks, M., and Markl, G. (2012) The sulfur speciation in S-bearing
759 minerals: New constraints by a combination of electron microprobe analysis and DFT
760 calculations with special reference to sodalite-group minerals. American Mineralogist, 97,
761 1653–1661.
762 Holm, P.M., Wilson, J.R., Christensen, B.P., Hansen, L., Hansen, S.L., Hein, K.M., Mortensen,
763 A.K., Pedersen, R., Plesner, S., and Runge, M.K. (2006) Sampling the Cape Verde Mantle
764 Plume: Evolution of Melt Compositions on Santo Antão, Cape Verde Islands. Journal of
765 Petrology, 47(1), 145–189.
766 Ibhi, A., Nachit, H., Abia, E.H., and Hernandez, J. (2002) Intervention des ségrégats
767 carbonatitiques dans la pétrogenèse des néphélinites à pyroxène de Jbel Saghro (Anti-Atlas,
768 Maroc). Bulletin de la Societe Geologique de France, 173, 37–43.
769 Johnson, M.C., Anderson, A.T., and Rutherford, M.J. (1994) Pre-eruptive volatile contents of
770 magmas. Reviews in Mineralogy and Geochemistry, 30, 281–330.
771 Jugo, P. (2009) Sulfur content at sulfide saturation in oxidized magmas. Geology, 37(5), 415–418.
772 Jugo, P.J., Wilke, M., and Botcharnikov, R.E. (2010) Sulfur K-edge XANES analysis of natural
773 and synthetic basaltic glasses: Implications for S speciation and S content as function of
774 oxygen fugacity. Geochimica et Cosmochimica Acta, 74(20), 5926–5938.
775 Klaudius, J., and Keller, J. (2006) Peralkaline silicate lavas at Oldoinyo Lengai, Tanzania. Lithos,
776 91, 173–190.

Laporte, D., Lambart, S., Schiano, P., and Ottolini. L. (2014) Experimental Derivation of Nepheline Syenite and Phonolite Liquids by Partial Melting of Upper Mantle Peridotites. Earth and Planetary Science Letters, 404, 319–31.

Legendre, C., Maury, R.C., Savanier, D., Cotton, J., Chauvel, C., Hemond, C., Bollinger, C., Blais, S., Guille, G., and Rossi. P. (2005) The Origin of Intermediate and Evolved Lavas in the Marquesas Archipelago: An Example from Nuku Hiva Island (French Polynesia). Journal of Volcanology and Geothermal Research, 143(4), 293–317.

Le Maitre, R.W. (1984) A Proposal by the IUGS Sub- Commission on the Systematics of Igneous Rocks for a Chemical Classification of Volcanic Rocks Based on the Total Alkali Silica (TAS) Diagram. Australian Journal of Earth Sciences, 31, 243–55.

Lemarchand, F., Villemant, B., and Calas, G. (1987) Trace element distribution coefficients in alkaline series. Geochimica et Cosmochimica Acta, 51(5), 1071–1081.

Lessing, P., and Grout, C.H. (1971) Haüynite from Edwards, New York. The American Mineralogist, 59, 1096–1100.

Luhr, J.F. (1990) Experimental Phase relations of Water- and Sulfur –Saturated Arc Magmas and the 1982 Eruptions of El Chichon Volcano. Journal of Petrology, 31(5), 1071–1114.

Masotta, M., Mollo, S., Freda, C., Gaeta, M., and Moore, G. (2013) Clinopyroxene-liquid thermometers and barometers specific to alkaline differentiated magmas. Contributions to Mineralogy and Petrology, 166, 1545–1561.

Mathez, E.A., and Webster, J.D. (2005) Partitioning behavior of chlorine and fluorine in the system apatite-silicate melt-fluid. Geochimica et Cosmochimica Acta, 69(5), 1275–1286.

McDonough, W.F., and Sun, S.-S. (1995) The composition of the Earth. Chemical Geology, 120, 223–253.

Mertes, H., and Schmincke, H.-U. (1985) Mafic potassic lavas of the Quaternary West Eifel volcanic field. Contributions to Mineralogy and Petrology, 89, 330–345.

Métrich, N., and Wallace, P. (2008) Volatile abundances in basaltic magmas and their degassing paths tracked by melt inclusions. Reviews in Mineralogy and Geochemistry, 69, 363–402.

Missenard, Y., and Cadoux, A. (2011) Can Moroccan Atlas lithospheric thinning and volcanism be induced by Edge-Driven Convection? Terra Nova, 00, 1–8.

Mollo, S., and Masotta. M. (2014) Optimizing Pre-eruptive Temperature Estimates in Thermally and Chemically Zoned Magma Chambers. Chemical Geology, 368, 97–103.

Mollo, S., Masotta. M., Forni, F., Bachmann, O., De Astis, G., Moore, G., and Scarlato, P. (2015) A K-feldspar-liquid hygrometer specific to alkaline differentiated magmas. Chemical Geology, 392, 1–8.

Morimoto, N. (1988) Nomenclature of pyroxenes. American Mineralogist, 73, 1123–1133.

Olin, P.H., and Wolff, J.A. (2012) Partitioning of rare earth and high field strength elements between titanite and phonolitic liquid. Lithos, 128-131, 46–54.

Oppenheimer, C., Moretti, R., Kyle, P., Eschenbacher, A., Lowenstern, J.B., Hervig, R.L., and Dunbar, N.W. (2011) Mantle to surface degassing of alkali magmas at Erebus volcano, Antartica. Earth and Planetary science letters, 306, 261–271.

Parat, F., and Holtz, F. (2005) Sulfur partition coefficient between apatite and rhyolite: the role of bulk S content. Contributions to Mineralogy and Petrology, 150, 643–651.

Parat, F., Holtz, F., and Feig, S. (2008) Pre-eruptive conditions of the Huerto Andesite (Fish Canyon System, San Juan Volcanic Field, Colorado): Influence of Volatiles (C-O-H-S) on phase equilibria and mineral composition. Journal of Petrology, 49(5), 911–935.

Parat, F., Holtz, F., and Klugel, A. (2011) S-rich apatite-hosted glass inclusions in xenoliths from La Palma: constraints on the volatile partitioning in evolved alkaline magmas. Contributions to Mineralogy and Petrology, 162, 463–478.

Parat, F., Holtz, F., and Streck, M.J. (2011) Sulfur-bearing Magmatic Accessory Minerals. Reviews in Mineralogy and Geochemistry, 73, 285–314.

Price, R.C., and Green. D.H. (1972) Lherzolite Nodules in a Mafic Phonolite from North East Otago, New Zealand. Nature, 235, 133–34.

Prowatke, S., and Klemme. S. (2006) Trace Element Partitioning Between Apatite and Silicate Melts. Geochimica et Cosmochimica Acta, 70, 4513–27.

Putirka, K. (2008) Thermometers and barometers for volcanics systems. Reviews in Mineralogy and Geochemistry, 69, 61–120.

Putirka, K.D., Mikaelian, H., Ryerson, F., and Shaw, H. (2003) New Clinopyroxene-liquid thermobarometers for mafic, and volatile-bearing lava composition, with applications to lavas from Tibet and the Snake river plain, Idaho. American Mineralogist, 88, 1542–1554.

Scaillet, B., and Pichavant, M. (2003) Experimental constraints on volatile abundances in arc magmas and their implications for degassing processes. Geological Society, London, Special Publications, 213, 23–52.

Scaillet, B., Pichavant, M., and Cioni, R. (2008) Upward migration of Vesuvius magma chamber over the past 20,000 years. Nature, 455, 216–219.

Schmidt, B.C., and Behrens, H. (2008) Water solubility in phonolite melts: Influence of melt composition and temperature. Chemical geology, 256, 259–268.

Schmincke, H.-U., Park, C., and Harms, E. (1999) Evolution and environmental impacts of the eruption of Laacher See Volcano (Germany) 12,900 a BP. Quaternary International, 61, 61–72.

Schnetzler, C.C., and Philpotts. J.A. (1970) Partition Coefficients of Rare-earth Elements Between Igneous Matrix Material and Rock-forming Mineral phenocrysts—II. Geochimica et Cosmochimica Acta, 34(3), 331–40.

Sharp, Z.D., Helffrich, G.R., Bohlen, S.R., and Essene, E.J. (1989) The stability of sodalite in the system $NaAlSiO_4$-NaCl. Geochimica et Cosmochimica Acta, 53, 1943–1954.

Signorelli, S., and Carroll, M.R. (2002) Experimental study of Cl solubility in hydrous alkaline melts: constraints on the theoretical maximum amount of Cl in trachytic and phonolitic melts. Contributions to Mineralogy and Petrology, 143, 209–218.

Signorelli S., Vaggelli, G., and Romano, C. (1999) Pre-eruptive volatile (H2O, F, Cl, and S) contents of phonolitic magmas feeding the 3550-year old Avellino eruption from Vesuvius, Southern Italy. Journal of Volcanology and Geothermal Research, 93(3-4), 237–256.

Stormer, J., and Carmichael, I.S.E. (1971) The free energy of sodalite and the behavior of chloride, fluoride and sulfate in silicate magmas. American Mineralogist, 56, 292–305.

Thompson, G.M., Smith, I.E.M., and Malpas, J.G. (2001) Origin of oceanic phonolites by crystal fractionation and the problem of the Daly gap: an example from Rarotonga. Contributions to Mineralogy and Petrology, 142, 336–346.

Tomisaka, T., and Eugster. H.P. (1969) Synthesis of the Sodalite Group and Subsolidus Equilibria in the Sodalite-noselite System. Journal of the Mineralogical Society of Japan, 5, 249–75.

Toulmin, P., and Barton, P. (1964) A thermodynamic study of pyrite and pyrrhotite. Geochimica et Cosmochimica Acta, 78, 641–671.

Trail, D., Watson, E.B., and Tailby, N.D. (2012) Ce and Eu anomalies in zircon as proxies for the oxidation state of magmas. Geochimica et Cosmochimica Acta, 97, 70–87.

Van Achterbergh, E., Ryan, C.G., and Griffin, W.L. (2001) GLITTER on-line interactive data reduction for the LA-ICPMS microprobe. Macquarie Research Ltd., Sydney.

Van Peteghem, J.K., and Burley. B.J. (1963) Studies on Solid Solution Between Sodalite, Nosean and Haüyne. The Canadian Mineralogist, 7, 808–13.

Vernet, M., Marin, L., Boulmier, S., Lhomme, J., and Demange, J.C. (1987) Dosage du fluor et du chlore dans les matériaux géologiques y compris les échantillons hyperalumineux. Analusis, 15(9), 490–498.

Webster, J.D., Goldoff, B., Sintoni, M.F., Shimizu, N., and De Vivo. B. (2014) C-O-H-Cl-S-F Volatiles Solubilities, Partitioning, and Mixing in Phonolitic-Trachytic Melts and Aqueous-Carbonic Vapor and Saline Liquid at 200 MPa. Journal of Petrology, 55(11), 2217–48.

Webster, J.D., Goldoff, B., and Shimizu, N. (2011) C-O-H-S fluids and granitic magma: how S partitions and modifies CO_2 concentrations of fluid-saturated felsic melt at 200 MPa. Contributions to Mineralogy and Petrology, 162, 849–865.

Webster, J.D., Sintoni, M.F., and De Vivo, B. (2009) The partitioning behavior of Cl, S, and H2O in aqueous vapor- ±saline-liquid saturated phonolitic and trachytic melts at 200 MPa. Chemical Geololy, 263, 19–36.

Wedepohl, K.H., Gohn, E., and Hartmann, G. (1994) Cenozoic alkali basaltic magmas of western Germany and their products of differentiation. Contributions to Mineralogy and Petrology, 115, 253–278.

Willemant, B. (1988) Trace element evolution in the Phlegrean Fields (Central Italy): fractional crystallization and selective enrichment. Contributions to Mineralogy and Petrology, 98, 169–183.

Whitney, J. (1984) Fugacities of sulfurous gases in pyrrhotite-bearing silicic magmas. American Mineralogist, 69, 69–78.

Wörner, G., Beusen, J.-M., Duchateau, N., Gijbels, R., and Schmincke, H.-U. (1983) Trace element abundances and mineral/melt distribution coefficients in phonolites from the Laacher See Volcano (Germany). Contributions to Mineralogy and Petrology, 84, 152–173.

Wörner, G., and Schmincke, H.-U. (1984a) Mineralogical and Chemical Zonation of the Laacher See Tephra Sequence (East Eifel, W. Germany). Journal of Petrology, 25(4), 805–835.

Wörner, G., and Schmincke, H.-U. (1984b) Petrogenesis of the zoned Laacher See Tephra. Journal of Petrology, 25(4), 836–851.

Zaitsev, A.N., Marks, M.A.W., Wenzel, T., Spratt, J., Sharygin, V.V., Strekopytov, S., and Markl, G. (2012) Mineralogy, geochemistry and petrology of the phonolitic to nephelinitic Sadiman volcano, Crater Highlands, Tanzania. Lithos, 152, 66–83.

Figure Captions

Figure 1. Alkali vs silica composition (after Le Maitre 1984) of the sodalite-bearing phonolites: haüyne-bearing phonolites (*white diamond and triangle:* this study, Wörner and Schmincke 1984a, Holm et al. 2006, and Bryan 2006); nosean-bearing phonolites (*black diamond and triangle:* this study, Berger et al. 2009, and Brousse et al. 1969); sodalite-bearing phonolite (*grey full circle*: Klaudius and Keller 2006 and Zaitsev et al. 2012); and nephelinite and basanite, Eifel *(white square:* Mertes and Schmincke 1985 and Wedepohl et al. 1994), nephelinite Saghro (*black square:* Berger et al. 2009).

Figure 2. Photomicrographs of phonolite from a) Laacher See and b) Saghro. *San* sanidine, *cpx* clinopyroxene, *ha* haüyne, *ne* nepheline, *nsn* nosean. Scale bar = 1 mm.

Figure 3. (a) Cl vs S content in Sodalite, (b) Composition of the sodalite group in phonolites recalculated to cation percentage (after Lessing and Grout 1971); symbols as in Figure 1.

Figure 4. REE content in (a) cpx, (b) haüyne (stripped zone: HREE concentration close to detection limit), (c) titanite, (d) apatite, and (e) plagioclase from Laacher See phonolite. Normalization values from McDonough and Sun (1995).

Figure 5. REE content in (a) cpx, (b) nosean (stripped zone: HREE close to detection limit), (c) titanite, and (d) apatite from Saghro phonolite. Grey= Laacher See phonolite. Normalization values from McDonough and Sun (1995).

928 Figure 6. P-T conditions calculated from cpx-liquid thermobarometer (Masotta et al.
929 2013) for Saghro and Laacher See phonolites.
930
931 Figure 7. Calculated liquid compositions in equilibrium with (a) cpx, (b) nosean, (c)
932 titanite, (d) apatite, and (e) plagioclase for Laacher See phonolite. Liquid composition
933 calculated using partition coefficients from Wörner et al. (1983), Olin and Wolff (2012),
934 Prowatke and Klemme (2006), and Francalanci et al. (1987). Whole rock and partition
935 coefficients from Wörner et al. (1983) are for sample 1088 from ULST. Normalization values
936 from McDonough and Sun (1995).
937
938 Figure 8. Calculated liquid compositions in equilibrium with (a) cpx, (b) haüyne, (c)
939 titanite, and (d) apatite for Saghro phonolite. Liquid composition calculated using partition
940 coefficients from Wörner et al. (1983), Olin and Wolff (2012), Prowatke and Klemme (2006),
941 Francalanci et al. (1987). Normalization values from McDonough and Sun (1995).
942
943 Figure 9. Sulfur and chlorine content in Saghro and Laacher See phonolites, melt
944 inclusions and liquid in equilibrium with apatite (S^{6+}). ULST Laacher See bulk rock data from
945 Wörner and Schmincke (1984a) and melt inclusions data from Harms et al. (2000).
946
947 Figure 10. Cu/Ni in minerals vs La/Sm ratio between bulk rock and liquid in equilibrium
948 with minerals. Full and open symbols for Saghro and Laacher See minerals, respectively.
949
950
951 **Tables**
952

Table 1. Major (wt%) and trace element (ppm) compositions of Saghro (TAG) and Laacher See (HE2) phonolite.

Sample	TAG	HE2
wt%		
SiO_2	52.79	58.72
TiO_2	0.84	0.51
Al_2O_3	19.87	20.38
$Fe_2O_{3\ tot}$	4.96	2.12
MgO	1.12	0.18
MnO	0.23	0.09
CaO	2.72	2.45
Na_2O	9.58	5.32
K_2O	6.75	8.77
P_2O_5	0.20	0.11
LOI	0.89	1.28
Total	99.95	99.93
Mg#	0.31	0.13
ppm		
C	130	391
S	560	4000
F	520	440
Cl	2530	820
Cr	44.6	4.8
Ni	15.7	2.2
Cu	5.9	7.0
Rb	234	102
Sr	1146	919
Y	21.8	5.85
Zr	1014	171
Nb	278	54.3
Ba	609	2052
La	70.9	32.3
Ce	108	56.1
Pr	8.8	5.0
Nd	28.1	15.1
Sm	4.2	1.80
Eu	1.4	0.98
Gd	3.4	1.58
Tb	0.6	0.21
Dy	3.7	1.11
Ho	0.8	0.25
Er	2.4	0.70
Tm	0.4	0.11
Yb	2.7	0.68
Lu	0.5	0.10
Hf	11.9	3.39
Ta	5.3	3.04
Pb	18.2	8.06
Th	35.8	5.06
U	12.5	1.05

$Mg\# = Mg/[Mg+Fe^{2+}]$

Table 2. Representative major element compositions (wt%) of mineral in Saghro (TAG) and Laacher See (HE2) phonolite.

Sample	TAG	TAG	HE2	HE2	TAG	HE2	HE2	TAG	HE2	TAG	HE2	TAG	TAG	HE2	HE2	TAG	TAG	HE2	TAG	He2
Mineral	cpx	cpx	cpx	cpx	tit	tit	am	ne	pl	san	san	nsn	nsn	ha	ha	ap	ap	ap	mt	mt
Type	core	rim	core	core	core	core	core	core	core	core	core	core	rim	core	core	in cpx	int	int	core	core
SiO_2	44.84	51.14	46.35	45.60	29.66	29.22	38.55	45.96	57.94	63.73	63.27	38.51	35.59	33.52	33.31	0.55	0.46	0.87	0.23	0.11
TiO_2	3.4	0.94	1.73	2.04	36.04	36.60	4.79	-	0.05	0.07	0.1	-	-	-	-	-	-	-	8.34	7.56
Al_2O_3	8.66	2.13	6.21	7.13	1.13	1.26	13.04	35.58	25.98	18.47	19.86	34.43	30.51	28.95	29.21	0.01	-	-	0.14	2.36
FeO^{tot}	6.24	13.65	11.42	11.31	1.59	1.22	16.14	0.76	0.35	0.79	0.17	0.30	0.52	0.21	0.18	0.12	0.07	-	88.59	86.69
MnO	0.1	0.77	0.69	0.62	0.06	0.13	0.61	b.d.	b.d.	b.d.	b.d.	-	-	0.02	0.02	0.04	0.03	0.09	1.58	1.84
MgO	12.06	8.44	9.74	9.44	0.02	0.02	9.30	0.01	0.02	b.d.	0.01	-	-	0.03	0.04	-	-	-	0.83	1.4
CaO	23.32	19.70	22.46	22.51	27.83	28.02	11.87	0.01	7.52	0.01	0.77	0.01	0.36	9.88	9.87	53.59	54.35	52.94	0.18	0.01
Na_2O	0.56	2.81	1.27	1.18	1.05	0.01	2.17	12.23	6.31	3.30	3.16	20.49	15.01	15.09	15.2	0.1	0.03	0.05	-	-
K_2O	b.d.	0.02	b.d.	b.d.	0.01	0.01	2.47	5.26	1.61	13.15	11.91	1.42	11.15	1.17	1.12	0.01	0.01	-	-	-
P_2O_5	-	-	-	-	-	-	-	-	-	-	-	0.07	0.23	0.01	0.03	40.36	41.24	41.91	-	-
Cr_2O_3	0.34	0.02	0.01	0.02	b.d.	b.d.	0.02	b.d.	0.01	-	-	-	-	-	-	-	-	-	0.05	0.02
SO_2	-	-	-	-	-	-	-	-	-	-	-	6.52	6.01	11.08	11.14	0.08	0.04	0.78	-	-
F	-	-	-	-	-	-	-	-	-	-	-	-	-	-	-	3.05	3.75	3.62	-	-
Cl	-	-	-	-	-	-	-	-	-	-	-	1.19	0.19	0.31	0.30	0.04	0.01	0.25	-	-
Total	99.5	99.6	99.88	99.85	97.8	96.51	98.96	99.85	99.79	99.52	99.25	102.9	99.65	100.3	100.4	97.97	99.29	99.79	100	100
S^{6+}/S^{tot}	-	-	-	-	-	-	-	-	-	-	-	0.87	0.87	0.91	0.91	-	-	-	-	-
Mg#	0.60	0.32	0.40	0.39	-	-	0.50	-	-	-	-	-	-	-	-	-	-	-	-	-
Numbers of ions on the basis of																				
	6 O				**5 O**		**23O**	**32O**	**8O**			**24O on Al+Si tetrahedrons**				**26 O**			**4O**	
Si	1.67	1.94	1.75	1.72	1.01	0.99	5.87	8.61	2.60	2.95	2.90	5.84	5.97	5.95	5.90	0.10	0.08	0.15	0.01	0.01
Al^{IV}	0.33	0.06	0.25	0.28	-	-	2.13	-	-	-	-	-	-	-	-	-	-	-	-	-
Al^{VI}	0.05	0.03	0.02	0.04	-	-	0.21	-	-	-	-	-	-	-	-	-	-	-	-	-
Al tot	-	-	-	-	0.05	0.05		7.87	1.38	1.01	1.07	6.16	6.03	6.05	6.10	-	-	-	0.01	0.12
Ti	0.10	0.03	0.05	0.06	0.92	0.94	0.55	-	-	-	-	-	-	-	-	-	-	-	0.28	0.25
Fe^{2+}	0.08	0.25	0.13	0.15	-	-	-	-	-	-	-	-	-	-	-	-	-	-	-	-
Fe^{3+}	0.11	0.18	0.23	0.21	-	-	-	-	-	-	-	-	-	-	-	-	-	-	-	-

Fe tot	-	-	-	-	0.05	0.03	2.05	0.12	0.01	0.03	0.01	0.04	0.06	0.03	0.02	-	-	-	3.29	3.15
Mn	-	0.02	0.02	0.02	-	-	0.08	-	-	-	-	-	-	-	-	0.01	-	0.01	0.06	0.07
Mg	0.67	0.48	0.55	0.53	-	-	2.11	-	-	-	-	0.00	0.00	0.00	0.01	-	-	-	0.06	0.09
Ca	0.93	0.80	0.91	0.91	1.01	1.02	1.94	-	0.36	-	0.04	0.00	0.06	1.60	1.59	10.20	9.92	9.70	0.01	-
Na	0.04	0.21	0.09	0.09	0.01	-	0.64	4.46	0.55	0.3	0.28	5.78	4.16	4.42	4.43	0.05	-	0.02	-	-
K	-	-	-	-	-	-	0.48	1.26	0.09	0.78	0.7	0.26	2.03	0.23	0.22	-	-	-	-	-
P	-	-	-	-	-	-	-	-	-	-	-	-	-	-	-	5.86	5.95	5.87	-	-
SO_4^{2-}	-	-	-	-	-	-	-	-	-	-	-	1.27	1.64	1.72	1.73	0.02	0.01	0.15	-	-
S^{2-}	-	-	-	-	-	-	-	-	-	-	-	0.19	0.24	0.17	0.17	-	-	-	-	-
Cl	-	-	-	-	-	-	-	-	-	-	-	0.53	0.12	0.11	0.10	-	-	0.02	-	-
OH	-	-	-	-	-	-	-	-	-	-	-	-	-	-	-	1.03	0.91	0.92	-	-
F	-	-	-	-	-	-	-	-	-	-	-	-	-	-	-	0.96	1.09	1.06	-	-
Total	4.00	4.00	4.00	4.00	3.03	3.04	16.00	22.32	5.00	5.00	5.00	20.07	20.11	20.27	20.27	18.23	17.96	17.89	3.70	3.70

b.d.—below detection, cpx—clinopyroxene, tit—titanite, am—amphibole, ne—nepheline, pl—plagioclase, san—sanidine, nsn—nosean, ha—haüyne, ap—apatite, int—interstitial, mt-magnetite

Table 3. Representative trace element compositions (ppm) of mineral for Saghro (TAG) and Laacher See (HE2) phonolite.

Sample	TAG	TAG	HE2	HE2	TAG	HE2	HE2	HE2	TAG	TAG	TAG	HE2	HE2	HE2	TAG	TAG	HE2	HE2
Mineral	cpx	cpx	cpx	cpx	tit	tit	pl	san	nsn	nsn	nsn	ha	ha	ha	ap	ap	ap	ap
Type	core	rim	core	core	core	core	core	core	core	core	rim	core	core	core	in cpx	int	int	int
Ni	3.1	-	0.6	0.5	0.3	2.7	1.94	3.6	1.6	0.6	5.43	0.8	0.7	0.8	0.9	6.1	1.9	1.9
Cu	0.2	-	0.1	0.2	2.6	1.3	0.36	2.37	31.1	6.4	59.9	0.2	0.2	2.2	0.3	3.9	0.9	0.59
Rb	b.d.	7	0.5	-	0.1	0.1	2.78	107	4.9	8.6	40.8	5.6	4.9	5.4	-	2.8	-	-
Ba	0.3	2.7	0.9	0.1	0.1	0.2	1384	4264	20.6	10.7	18.4	21.3	20.7	26.7	23.6	15.3	2.2	1.6
Th	0.3	1.3	0.2	0.1	54.2	124	0.03	0.56	0.3	0.3	3.26	b.d.	-	b.d.	85	109	107	86.9
U	b.d.	0.2	b.d.	b.d.	8.8	16	b.d.	0.03	0.1	0.1	4.21	-	-	-	6.9	13.9	8.4	7.3
Nb	3.9	13.9	4.9	3.8	5863	9128	0.07	3.6	3.5	3.3	19.4	0.6	0.6	0.5	6.7	3303	0.9	0.9
Ta	0.8	0.5	0.6	0.4	325	583	b.d.	b.d.	b.d.	b.d.	0.1	b.d.	b.d.	b.d.	-	178	-	-
Pb	0.1	0.2	0.3	0.2	0.3	1.2	3.28	7.2	16.2	3.7	75.3	1.1	1.1	1.1	2.9	7.5	1.3	1.3
Sr	570	278	66.5	39.6	1388	5	2609	1725	303	268	1153	492	461	474	10942	9880	852	872
Zr	319	137	358	318	1706	5722	0.27	10.9	5.7	1.4	22.5	0.1	0.1	0.1	4.6	1156	14.5	12.8
Hf	9.1	5.5	10.6	9.2	37.5	172	b.d.	0.11	b.d.	b.d.	0.35	b.d.	-	b.d.	-	25.9	-	-
Y	21.3	14.9	35.1	33.7	543	954	0.24	0.73	0.5	0.7	1.62	0.5	0.5	0.5	330	588	555	528
La	23.6	14.3	41.4	38.6	1505	4035	21.9	9.5	5.4	8.9	6.39	11.6	11.5	11.9	2808	3204	3320	3150
Ce	65.5	39.6	116	112	3699	9041	22.5	6.2	8.9	13.2	6.21	17.5	17.1	17.9	3939	5703	6345	5774
Pr	9.32	5.94	15.2	14.7	427	928	1.43	0.45	0.7	1.1	0.77	1.5	1.4	1.5	331	542	580	550
Nd	42.9	28.7	60	55.7	1505	2469	3.2	1.3	2.1	3.1	2.23	3.9	3.9	3.9	1045	1786	1898	1771
Sm	9.4	6.8	9.8	8.9	237	290	0.24	0.20	0.2	0.3	0.27	0.3	0.3	0.3	139	242	206	192
Eu	2.9	2.1	2.3	2.1	66	44.1	0.74	0.71	b.d.	b.d.	0.09	0.2	0.2	0.2	39.2	65.6	43	40.8
Gd	7.5	5.9	7.9	7.1	186	208	0.17	0.40	0.2	0.3	0.27	0.2	0.3	0.2	115	190	169	157
Tb	1.0	0.7	1	1	24.4	29.2	0.01	b.d.	b.d.	b.d.	0.03	b.d.	0.2	0.2	11.6	23	18.7	16.7
Dy	5.3	3.8	6.9	6.5	132	168	0.03	0.12	0.1	0.1	0.19	0.1	0.1	0.1	65	133	105	96.1
Ho	0.8	0.6	1.3	1.3	21.2	33.1	b.d.	0.15	b.d.	b.d.	0.03	b.d.	b.d.	b.d.	11.2	21.7	19.4	18.3
Er	1.9	1.3	3.8	3.7	49.5	102	b.d.	0.04	b.d.	b.d.	0.11	b.d.	b.d.	b.d.	29.1	53.1	52.4	48.4
Tm	0.2	0.2	0.6	0.5	6.1	14.4	b.d.	b.d.	b.d.	b.d.	0.02	b.d.	b.d.	b.d.	3.3	6.7	6.7	6.1
Yb	1.5	0.9	4.5	4.3	31.4	88.6	b.d.	b.d.	b.d.	b.d.	b.d.	b.d.	b.d.	b.d.	18.1	32.7	38.6	36.8
Lu	0.2	0.1	0.8	0.7	3.1	10	b.d.	b.d.	b.d.	b.d.	b.d.	b.d.	b.d.	b.d.	2.1	3.4	5.0	4.9

b.d.—below detection, cpx—clinopyroxene, tit—titanite, pl—plagioclase, san—sanidine, nsn—nosean, ha—haüyne, ap—apatite, int—interstitial

963

Table 4. Representative major and trace element composition of pyrrhotite.

Sample	TAG	TAG	TAG	HE2	HE2	HE2
Mineral	po	po	po	bornite	po	po
Type	int	int	in cpx	in cpx	in mt	in cpx
wt%						
Fe	60.06	60.05	53.03	14.46	57.93	58.86
S	37.41	37.4	38.77	25.34	38.55	38.31
Cu	1.84	1.07	<0.01	60.78	0.37	0.30
Ni	0.85	1.38	0.04	0.03	<0.01	0.01
Total	100.1	99.9	92.8	100.5	96.85	97.48
N_{FeS}	0.96	0.97	0.9	-	0.92	0.93
ppm						
As	940	1162	6	100	19.4	7.9
Se	<19.6	32.6	50	541.7	19.9	15.1
Te	2.3	1.9	1.4	9.4	3.2	3.6
Pb	462.0	207.0	15.5	59.1	2.2	1.7
Bi	2.4	0.1	0.03	0.6	<0.1	<0.1
Ag	18.3	40.5	61.2	6.1	0.6	0.65
ppb						
Os	6	(7.5)	30	410	158	23.6
Ir	(2.6)	1.4	30	87	41	6.2
Ru	60	260	230	1360	150	440
Rh	230	96	80	1380	66	129
Pt	(18.0)	10	30	270	27	14
Pd	1900	300	920	n.d.	2300	1700
Au	100	60	100	1400	60	30
Re	60	50	120	50	n.d.	n.d.
Cu/Ni	2.2	0.8	0.05	55.3	89.4	24.6
Pd/Ir	711	185	30.6	933	14.8	120
S/Se	25400	15424	8000	615	18139	23857
Se/Te	8.40	16.7	35.7	57.8	6.2	4.1

NFeS = fraction of FeS (Toulmin & Barton, 1964), concentration under detection limit in paranthesis; po—pyrrhotite, int—interstitial, cpx—clinopyroxene, mt—magnetite

964

965

Baudouin and Parat 2015

Figure 1

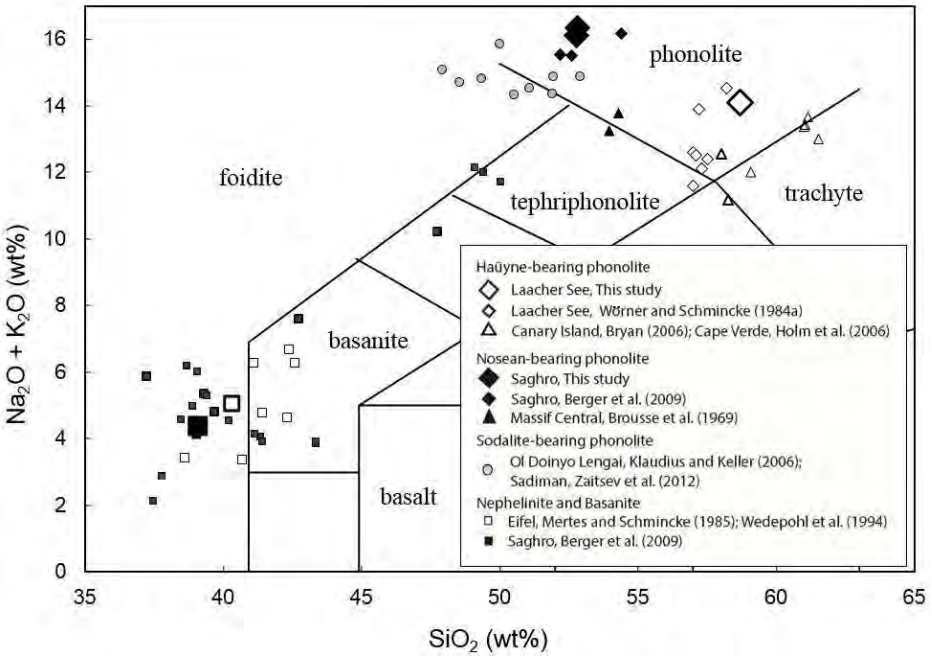

Baudouin and Parat 2015

Figure 2

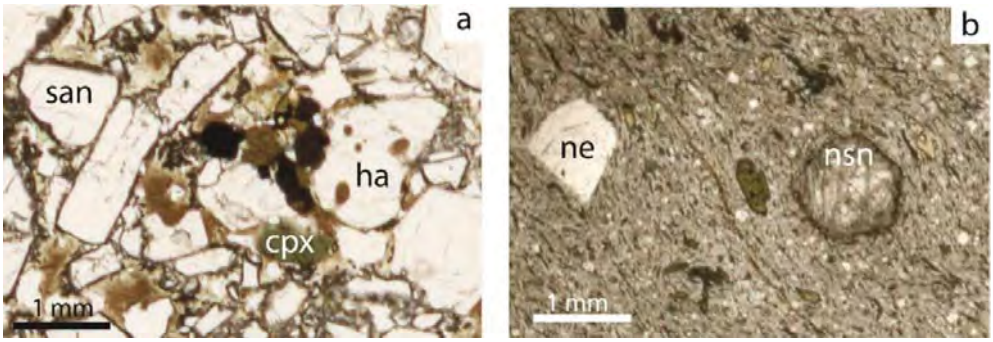

Baudouin and Parat 2015

Figure 3

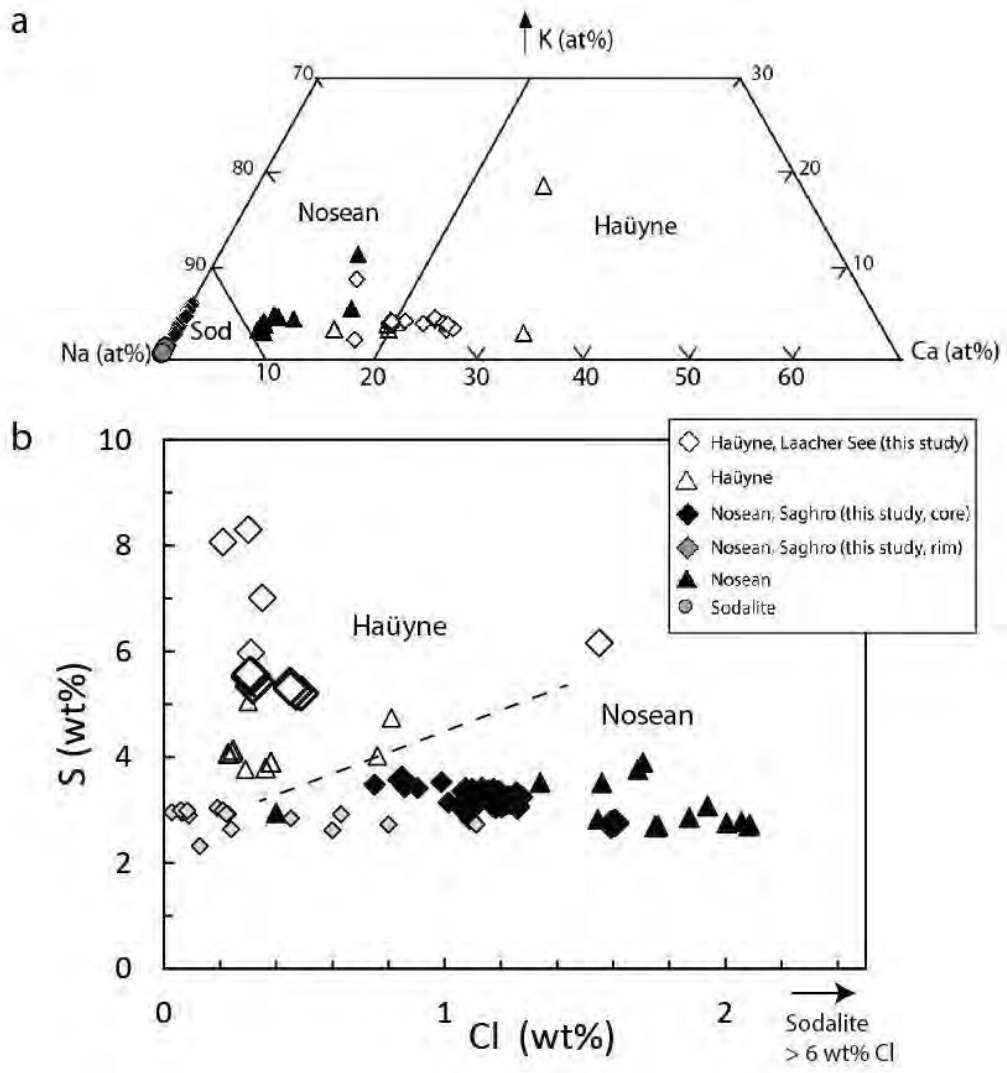

Baudouin and Parat 2015

Figure 4

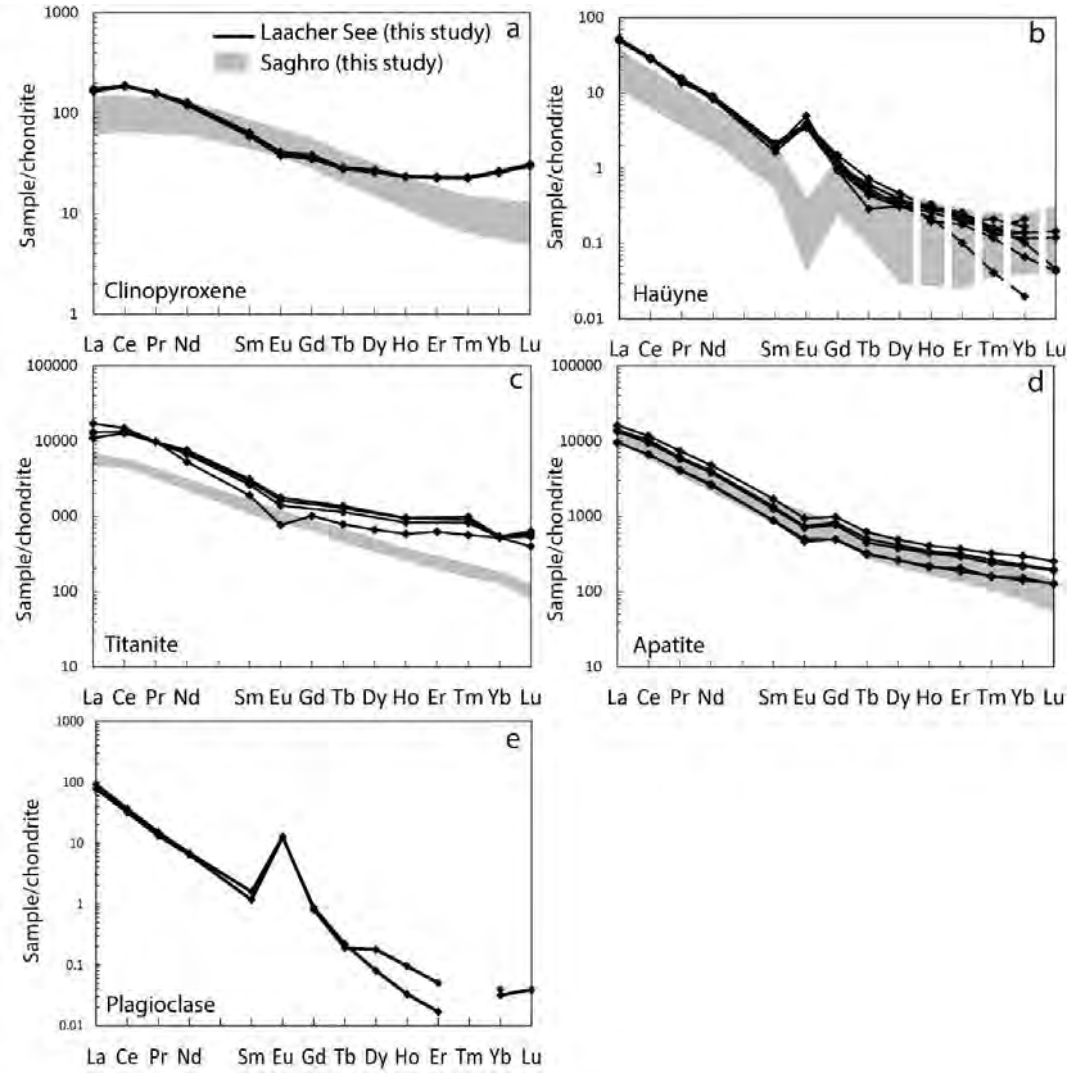

Baudouin and Parat 2015

Figure 5

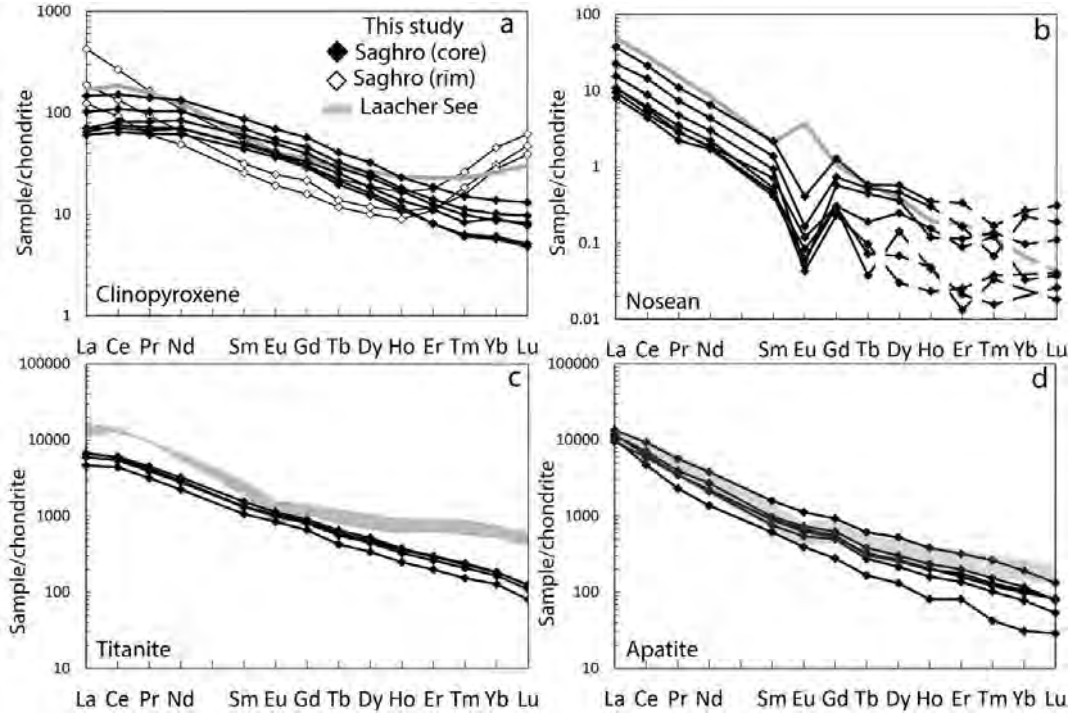

Baudouin and Parat 2015

Figure 6

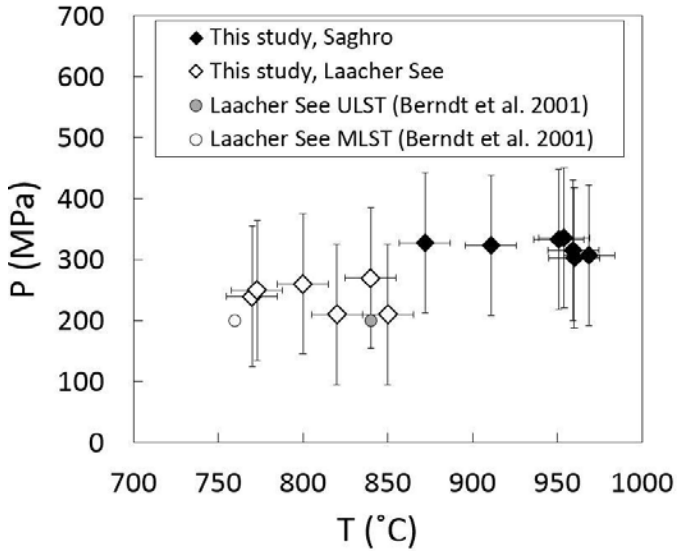

Baudouin and Parat 2015

Figure 7

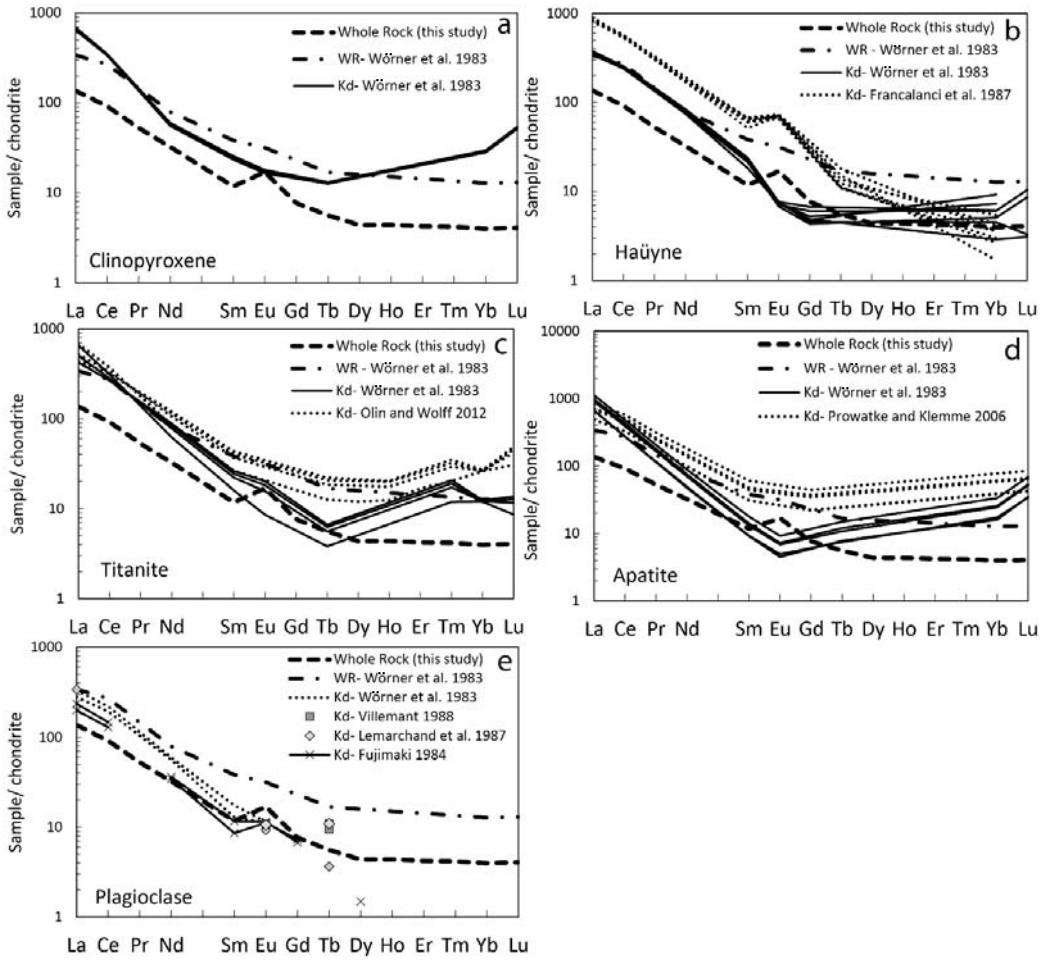

Baudouin and Parat 2015

Figure 8

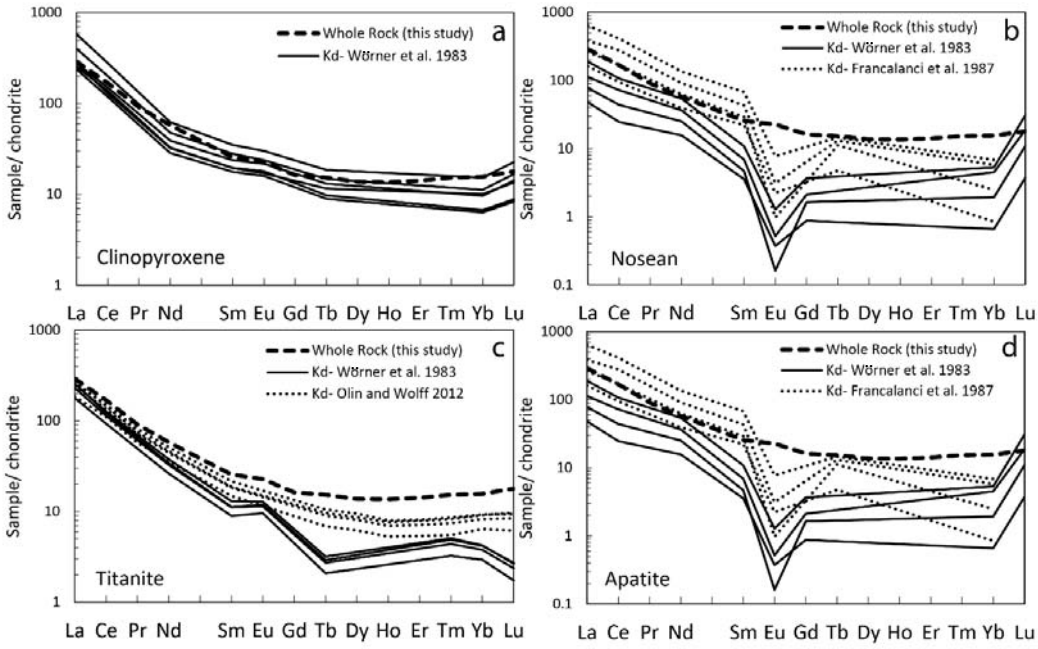

Baudouin and Parat 2015

Figure 9

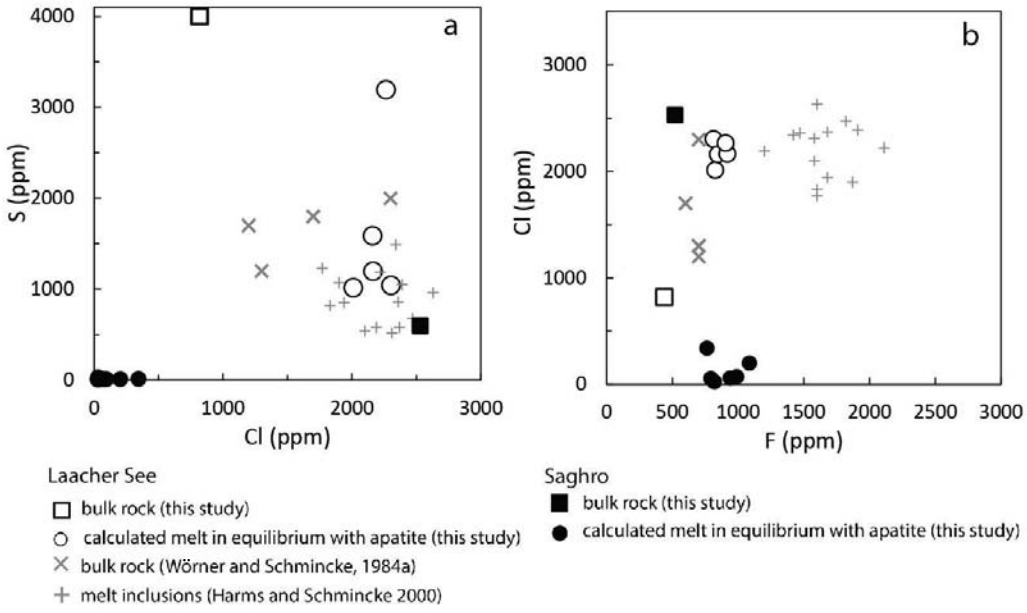

Baudouin and Parat 2015

Figure 10